To unravel the interaction between Nup155 and Nup93 via structural studies

A Thesis

submitted to

Indian Institute of Science Education and Research Pune in partial fulfilment of the requirements for the BS-MS Dual Degree Programme

by

Suyog Zinjurte (20191200)

Indian Institute of Science Education and Research Pune

Dr. Homi Bhabha Road,

Pashan, Pune 411008, INDIA.

Date: 17 May, 2024

Under the guidance of

Supervisor: Dr. Radha Chauhan,

NCCS Pune

From May 2023 to March 2024

INDIAN INSTITUTE OF SCIENCE EDUCATION AND RESEARCH PUNE

Certificate

This is to certify that this dissertation entitled “To unravel the interaction between Nup155 and Nup93 via structural studies” towards the partial fulfilment of the BS-MS dual degree programme at the Indian Institute of Science Education and Research, Pune represents work carried out by Suyog Zinjurte at National Centre for Cell Science (NCCS), Pune under the supervision of Dr. Radha Chauhan, Scientist-F, during the academic year 2023-2024.

Dr. Radha Chauhan

Scientist-F, NCCS

Name of your Guide: Dr. Radha Chauhan

Name of Your TAC : Dr. Gayathri Pananghat

This thesis is dedicated to you, thank you for reading!

Declaration

I hereby declare that the matter embodied in the report entitled “To unravel the interaction between Nup155 and Nup93 via structural studies” are the results of the work carried out by me at National Centre for Cell Science, Pune, under the supervision of Dr. Radha Chauhan, and the same has not been submitted elsewhere for any other degree. Wherever others contribute, every effort is made to indicate this clearly, with due reference to the literature and acknowledgement of collaborative research and discussions.

Suyog Zinjurte

20191200

19th May 2024

Table of Contents

Declaration **3**
Abstract **9**
Acknowledgements **10**
Abbreviations **11**
Contributions **12**
1. Introduction **13**
1.1 Nuclear Pore complex and its role in eukaryotic cells 13
1.2 Architecture of nuclear pore complex 14
1.3 Inner ring complex and its function 16
1.3.1 Nucleoporin93 16
1.3.2 Nucleoporin155 17
1.4 The complex formation of Nucleoporin155 and Nucleoporin93 18
1.5 Prediction of interaction interface of Nup155 and Nup93 using CoRNeA tool 19
1.6 Rationale of the study 20
1.7 Objectives of the thesis 21
2. Material and methods **22**
2.1 Transformation of plasmids in BL21 DE3 (RIL) cells 22
2.1.1 For $Nup155^{1-515}$ and $Nup93^{599-819}$ 22
2.1.2 For $Nup155^{864-1391}$ and $Nup93^{1-819}$ 23
2.2 Affinity purification 23
2.2.1 Co-mixing experiment for $Nup155^{1-515}$.$Nup93^{599-819}$ complex purification 24
2.2.2 Co-mixing experiment for $Nup155^{864-1391}$.$Nup93^{1-819}$ by GST affinity strategy 24
2.2.3 Purification of $Nup155^{864-1391}$.$Nup93^{1-819}$ by GST anti-GFP nanobody 24
2.3 Size exclusion chromatography 25
2.3.1 Size exclusion chromatography for $Nup155^{1-515}$.$Nup93^{599-819}$ 27
2.3.2 Size exclusion chromatography for $Nup155^{864-1391}$.$Nup93^{1-819}$ 27
A) After GST affinity chromatography 27
B) After the On-bead thrombin digestion 27
C) Co-mixing experiment followed by SEC 27
D) GST affinity followed by SEC in the presence of DDM 28
2.4 SDS-Polyacrylamide gel electrophoresis 28
2.5 Western blotting 28
2.6 Buffer exchange of protein 29
2.7 Cross-linking experiments 29
2.8 Cryo-electron microscopy of protein 30
2.9 Cryo-EM data processing 30
3. Results **31**
3.1 Purification standardisation of $Nup155^{1-515}$.$Nup93^{599-819}$ 31
3.1.1 Interaction of $Nup155^{1-515}$.$Nup93^{599-819}$ 31
3.1.2 SDS-PAGE gel profiles of $Nup155^{1-515}$ and $Nup93^{599-819}$ 32

3.1.3 Standardisation of the parameters in purification....33
A) Optimisation of bead binding incubation time....33
B) Optimisation of post-induction incubation time....34
C) Optimisation of lysis buffer volume....35
3.1.4 Co-mixing strategy to increase yield....36
3.1.5 Optimisation of the yield of the complex $Nup155^{1-515}$.$Nup93^{599-819}$....36
3.1.6 Size exclusion chromatography of $Nup155^{1-515}$.$Nup93^{599-819}$....38
3.2 Purification standardisation of $Nup155^{864-1391}$.$Nup93^{1-819}$....39
3.2.1 Validation of interaction of $Nup155^{864-1391}$.$Nup93^{1-819}$....39
A) By GST affinity method....39
B) By Ni-NTA affinity method....40
C) By Size exclusion chromatography....41
D) GST tag digestion followed by size exclusion chromatography....42
E) By Co-mixing....42
E.1) Co-mixing purified proteins....42
E.2) Co-lysing of pellets....44
3.2.2 Buffer optimisation for $Nup155^{864-1391}$.$Nup93^{1-819}$....44
A) Use of DDM in the lysis and elution buffer....44
B) Purification by GST tagged anti-GFP nanobody....45
C) Stability check for protein complex....47
D) Cross-linking of the complex....47
3.2.3 Cryo-EM data processing....48
4. Discussion and Future prospects....50
5. References....51

List of Tables

Table 1 GST lysis buffer composition

Table 2 Ni-NTA binding buffer composition

Table 3 Optimised conditions for purification of Nup155$^{1-515}$.Nup93$^{599-819}$

List of Figures

Figure 1. Molecular architecture of NPC and different Nups.

Figure 2. Domain organisation and Alphafold predicted structures of Nup155 and Nup93

Figure 3. Segmentation maps of Nup155 and Nup93.

Figure 4. Convolution score for different regions of *Hs*Nup93 and *Hs*Nup155.

Figure 5. Constructs containing genes of $Nup93^{599-819}$ and $Nup155^{1-515}$.

Figure 6. Constructs containing genes of $Nup93^{1-819}$ and $Nup155^{864-1391}$.

Figure 7. Purification strategy by GST tagged anti-GFP nanobody

Figure 8. Confirmation of interaction for complex $Nup155^{1-515}$.$Nup93^{599-819}$.

Figure 9. Analysis of proteins in the complex by SDS-PAGE and western blotting.

Figure 10. Standardisation of bead binding incubation time.

Figure 11. Standardisation of post-induction incubation time.

Figure 12. Standardisation of lysis buffer volume.

Figure 13. Co-mixing experiment of $Nup155^{1-515}$.$Nup93^{599-819}$.

Figure 14. Affinity chromatography from 4 Litre culture volume.

Figure 15. Standardisation of buffer exchange for $Nup155^{1-515}$.$Nup93^{599-819}$.

Figure 16. Size exclusion chromatography for the $Nup155^{1-515}$.$Nup93^{599-819}$.

Figure 17. GST Affinity showing $Nup155^{864-1391}$ and $Nup93^{1-819}$ in the complex.

Figure 18. Purification with Ni-NTA affinity showing $Nup155^{864-1391}$.$Nup93^{1-819}$ in the complex.

Figure 19. Confirmation after size exclusion chromatography for $Nup155^{864-1391}$.$Nup93^{1-819}$ purified with GST affinity.

Figure 20. Size exclusion chromatography for $Nup155^{864-1391}$.$Nup93^{1-819}$ after on-bead thrombin digestion.

Figure 21. Purification of the complex by co-mixing.

Figure 22. Standardisation of buffer exchange for Nup155$^{864-1391}$.Nup93$^{1-819}$ with DDM.

Figure 23. Affinity purification using GST tagged anti-GFP nanobody.

Figure 24. Stability check for the protein complex.

Figure 25. Cross-linking assay for the Nup155$^{864-1391}$.Nup93$^{1-819}$.

Figure 26. Cryo-EM data processing.

Abstract

The nuclear pore complex is a necessary protein assembly in the cell that regulates the trafficking between the nucleus and cytoplasm. This megadalton assembly consists of multiple subunits known as nucleoporins, which assemble themselves to form submodules. Owing to the huge size and technical limitations, the basic structural architecture and functional understanding of this complex is limited. The other way to comprehend the function of the nuclear pore complex is to delineate the interactions among individual proteins and their subcomplexes and hence, study their structure. In this study we investigated the interaction between the two critical proteins of the inner ring - Nup93 and Nup155. Various domains of these two proteins were reconstituted in-vitro using bacterial expression system. Purification optimisation was performed to further stabilise these interactions and obtain high yield. From this study, we were able to reconstitute the domains of Nup155 with its interacting partner Nup93 and also collected cryo-EM data for the complex. We performed some initial data processing, from which we have concluded that the quality of the data is good enough, and can be used for further processing. In future, we will be aiming for a high resolution structure of the Nup155.Nup93 complex by processing the data we have collected. The high-resolution structure of the complex can be used as a small piece in the big LEGO puzzle, which will ultimately contribute to better understanding of the NPC.

Acknowledgements

First of all, I would like to thank my guide, Dr. Radha Chauhan, for allowing me to carry out the work. Your constant guidance and the discussions in the meetings helped me a lot to carry out my research work. My expert Dr. Gayathri Pananghat for constant support, critical review, and suggestions for the work. Jyotsana helped me to carry out the experimental work in the lab. Also, with the continuous discussion on setting up the new experiments. The discussion of the results with her, helped me a lot in carrying out my MS thesis. Also, I want to thank Aswathy, for clearing any small doubts and her help with both the experimental and computational work. I would also like to thank to all lab members including Dr. Priyanka, Dr. Krishnakant, Krishna, Bheem, Lalit, Javed for their suggestions during the lab meetings. I want to thank all my friends and family.

Abbreviations

Cryo-EM - Cryogenic electron microscopy

DNA - Deoxyribonucleic acid

EDTA - Ethylene diamine tetraacetic acid

EMD - Electron Microscopy Data

GDP - Guanosine diphosphate

GFP - Green Fluroscent Protein

GTP - Guanosine triphosphate

GST - Glutathione S-transferase

HRP - Horseradish peroxidase

HPLC - High-performance liquid chromatography

IR - Inner Ring

IPTG - Isopropyl β- d-1-thiogalactopyranoside

kDa - kilodalton

LB - Luria Broth

MDa - Megadalton

Ni-NTA - Nickel-nitrilotriacetic acid

NPC - Nuclear Pore Complex

PAGE - Polyacrylamide gel electrophoresis

PDB - Protein Data Bank

PBS - Phosphate buffered saline

PBST - Phosphate buffered saline with tween

plDDT - predicted local distance difference test

RNA - Ribonucleic acid

Rpm - Rotation per minute

SDS - Sodium dodecyl sulfate

SUMO - Small ubiquitin-related modifier

Contributions

Contributor name	Contributor role
RC	Conceptualization Ideas
RC	Methodology
-	Software
RC, JS	Validation
-	Formal analysis
SZ	Investigation
RC	Resources
SZ	Data Curation
SZ	Writing - original draft preparation
SZ, JS, ALB, RC	Writing - review and editing
RC	Visualisation
RC	Supervision
RC	Project administration
RC	Funding acquisition

RC - Dr. Radha Chauhan, SZ - Suyog Zinjurte, JS - Jyotsana Singh, ALB - Aswathy LB, GP - Dr. Gayathri Pananghat

1. Introduction

1.1 Nuclear Pore complex and its role in eukaryotic cells

A unique feature of eukaryotic cells is the presence of a distinct compartment called the nucleus. It functions by protecting the genomic DNA from external attack as well as helps in gene regulation. The entire nucleus is protected from the outside by a double-layered membrane, which regulates the trafficking through its specialised pore structures known as Nuclear Pore Complexes (NPCs). It allows the transport between the nucleus and cytoplasm, primarily macromolecules such as messenger RNAs and proteins. This ~110 MDa complex facilitates the free diffusion of less than ~40 kDa, whereas the more giant molecules are transported via facilitated or active transport. There are nearly ~500 such NPCs present in a single cell (Michael J Matunis, 2002; Aitchison et al., 2000).

The NPC channel is enriched with hydrophobic amino acids containing proteins, primarily composed of repeated units of phenylalanine and glycine residues, which creates a hydrophobic environment essential for transport. This acts as a permeability barrier in the NPC (Denning et al., 2003). The primary nuclear transporter is karyopherin-β's. These include importins, exportins, and bidirectional kap-β also. Ran, a small ras-like protein, helps the kap-β for the transport. Ran is present in two states; one is GTP bound, and the other is GDP bound. The GDP-bound state in the cytoplasm and GTP-bound state in the nucleus of ran protein is maintained by RanGAP and RCC1, respectively. Importin binds to the cargo in the cytoplasm and carries it to the nucleus. Inside the nucleus, the importin binds to GTP and releases the cargo molecule in the nucleus. Subsequently, both importin and GTP are recycled. Similarly, for the export, RanGTP binds to the cargo-bound exportin and this complex is released in the nucleus upon conversion of RanGTP to RanGDP in the cytoplasm (Izaurralde et al., 1997, Rexach and Blobel, 1995, Matsuura, 2016).

In addition to being part of nucleocytoplasmic trafficking, the NPCs have been shown to modulate the activity of sumoylating proteins, thus by regulating the SUMO pathway**.** The NPCs are also involve in other functions in the cell such as chromatin organisation, cell cycle, cytoskeletal organisation, 3D genome architecture, etc (Palancade and Doye, 2008, Sakuma and D'Angelo, 2017). Individual nucleoporins

have also been studied in the field and shown to be involved in different tissue-specific functions, making them very important in the development of an organism. For example, a heterozygous mutation in Nup155 has been associated with atrial fibrillation and sudden death (Zhang et al., 2008). Also, different mutations in the nucleoporins and their corresponding phenotypes have been studied in mice, which clearly stated the role of each Nups in the development of an organism. The mutations in different Nups have shown to be associated with many diseases such as Alzheimer's disease, Huntington's disease and are involved in the progression of cancer (Sakuma and D'Angelo, 2017). Several nucleoporins have demonstrated to be involved in mitosis, with the reports suggesting the localisation of the vertebrate Nup107-160 complexes in the kinetochore (Nakano et al., 2011, Belgareh et al., 2001). Moreover, incomplete depletion of either ELYS or Nup133 resulted in defects in cytokinesis in human cells, while depletion of the Seh1 subunit induced mitotic delay (Nakano et al., 2011, Zuccolo et al., 2007, Rasala et al., 2008).

1.2 Architecture of nuclear pore complex

The nuclear pore complex consists of 3 basic submodules: cytoplasmic filaments and ring which faces towards the cytoplasm, scaffold central channel embedded in the membrane, nuclear ring and the basket that faces towards the nucleus. In humans, these submodules are made up of 34 distinct nucleoporins in numerous copies, making up to a total of ~1000 protein subunit assembly. The NPC has an octa-core symmetry (Lin and Hoelz, 2019). Most of the proteins are present in a copy number of 32 in the NPC, except a few having lower or higher copy numbers. These proteins, collectively referred to as nucleoporins (Nups), are identified by their respective molecular weights (Ori et al., 2013). These proteins are placed in the NPC as submodules which include: the outer ring complex, inner ring complex, cytoplasmic filament complex and nuclear basket complex. The outer ring complex serves as the structural scaffold. This complex has 10 proteins: Sec13, Seh1, Nup96, Nup75, Nup160, Nup107, Nup37, Nup133, Nup43, and ELYS (Michael J Matunis, 2002). By negative stain EM, it has been revealed that these proteins are arranged in the shape of the alphabet 'Y'; due to that, this whole subunit is called the Y subcomplex (Lutzmann et al., 2002, Bui et al., 2013). Sandwiched between two outer rings, the inner ring subcomplex is present, which

contains Nup53, Nup155, Nup93, Nup188, Nup205, Nup98 and the channel nucleoporin heterotrimer Nup54, Nup62, Nup58 (Lin et al., 2016). Among these members, the Nup155 directly interacts with the membrane by attaching the inner ring layer to the membrane. Nup93, with the help of Nup188, Nup205 holds the channel nucleoporin heterotrimer in place. Channel nucleoporin heterotrimer regulates the transport within the NPC by restricting the macromolecules by creating a mesh like structure with the help of FxFG repeat domain of these proteins (Denning et al., 2003). The nuclear basket Nups consists of Tpr and Nup153 and Nup50 in humans, which are present in the nuclear side of the NPC. These Nups interact with the nucleocytoplasmic machinery and also regulate chromatin modification (Jarnik and Aebi, 1991, von Appen et al., 2015). A distinct category of Nups known as transmembrane Nups including NDC1, POM121, GP210 and TMEM33 are the linker proteins, which attach the whole NPC to the nuclear envelope (Michael J Matunis, 2002).

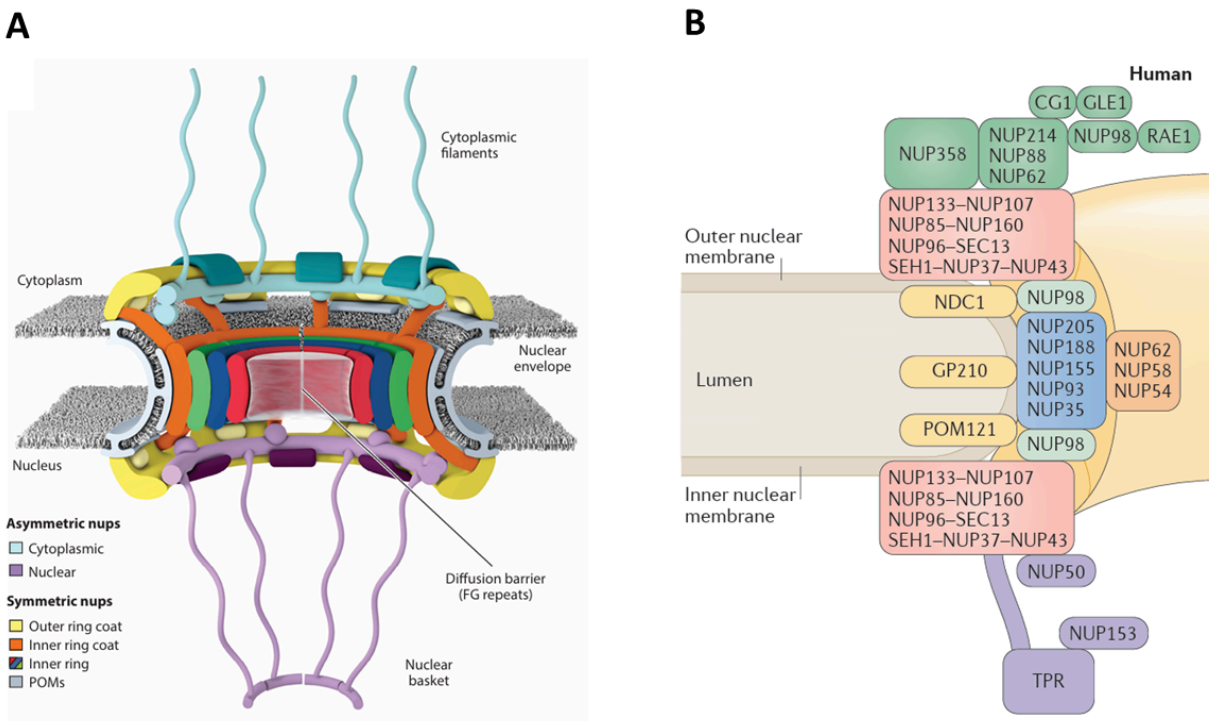

Figure 1. Molecular architecture of NPC and different Nups. (A) Different submodules of the NPC (adapted from Lin and Hoelz, 2019) (B) Different nucleoporins associated with each subcomplex. (adapted from Martin Beck and Ed Hurt, 2017)

1.3 Inner ring complex and its function

Among the 3 subunits, Inner ring (IR) occupies the middle position and connects the cytoplasmic ring (CR) and nuclear ring (NR). The Nups in the IR make a scaffold to which channel nucleoporin heterotrimer (CNT) adheres. During the cargoes transport, the concomitant rearrangement of IR Nups are essential for the process to proceed smoother. There are five different nucleoporins in the IR of higher eukaryotes, namely Nup205, Nup188, Nup93, Nup155, and Nup35. To form the inner ring, Nup155 forms the coat near the membrane, and the trimer Nup205-Nup188-Nup93 forms the inner layer and the CNT adheres to it, as shown in the tomography map from *X. laevis* (Huang et al., 2022). Similarly, the cryo-electron tomography map of the human inner ring has revealed that the total copy number for Nup93 and Nup62 is 32 each. Additionally, there are a combined total of 32 copies of Nup205 and Nup188, and 48 copies of Nup155, with 16 of them connecting to the outer rings (von Appen et al., 2015, Kosinski et al., 2016). Notably, Nup98 is present in 48 copies across the NPC to act as the linker protein and connect the IR to the adjacent rings (Ori et al., 2013).

1.3.1 Nucleoporin93

Nup93 is a highly versatile protein among the nucleoporins in the IR. It has multiple interacting partners in the different modules of the NPC. Its homologue is known as Nic96 in *S. cerevisiae*. It has been shown that the binding of the N-terminal of the Nic96 to the CNT is crucial for the formation of a diffusion barrier and, thus, for the active transport (Stuwe et al., 2015). Although the full length structure is not known, the structure of the human Nup93$^{174-819}$ domain has been solved recently by X-ray crystallography with 2.0 Å resolution (Petrovic et al., 2022). The N-terminal 1-96 region has high flexibility, which has shown low plDDT score by the Alphafold prediction (Jumper et al., 2021). At the C-terminal of Nup93 lies an alpha-solenoid domain, as depicted in Figure 2 A showing the domain organization.

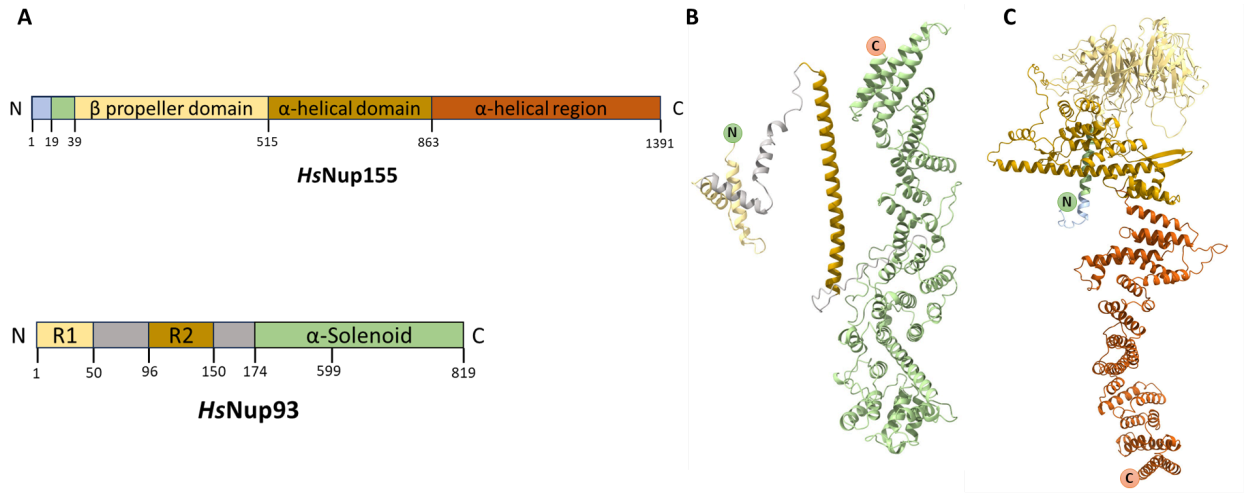

Figure 2. Domain organisation and Alphafold predicted structures of Nup155 and Nup93. (A) Domain organisation of *Hs*Nup155 and *Hs*Nup93, (B) Alphafold predicted structure of *Hs*Nup93 (Jumper et al., 2021) (C) Alphafold predicted structure of *Hs*Nup155 (Jumper et al., 2021). Colour coded as domain colour, visualised in Chimerax

1.3.2 Nucleoporin155

The Nup155 is present in the Inner ring complex of the NPC. In the lower eukaryotes, it has two homologues - Nup170 and Nup157. It has a membrane binding motif ALPS present in the β-propeller domain, by which it interacts with the nuclear membrane, shown in *Xenopus laevis* and in humans (Huang et al., 2022, Kosinski et al., 2016). Nup155 has a seven-bladed β-propeller domain in the N-terminal and an alpha-helical in the C-terminal (Figure 2). In the single-particle cryo-EM structure, the protein was found broken on the grid, and the structure was solved for the N-terminal Nup155$^{19\text{-}863}$ and C-terminal Nup155$^{864\text{-}1337}$ separately at a resolution of 5.2 Å and 5.3 Å respectively (Sangeeta Niranjan et al., 2021). The full-length Alphafold predicted structure is shown in (Figure 2 C). The mutation of R391H in Human Nup155 is associated with atrial fibrillation and sudden death (Zhang et al., 2008).

1.4 The complex formation of Nucleoporin155 and Nucleoporin93

According to the cryo-electron tomogram of the *Xenopus laevis* Inner ring, the Nup93 is present in 4 copies and the Nup155 is present in the 6 copies. The reported PDB (7WKK), shows the Nup155 and Nup93 are present in 4 conformations. In this structure, two copies of β-propeller regions of Nup155 are in close proximity to the nuclear membrane. In the middle, Nup93–Nup188–Nup205 forms the central scaffold, with the help of 4 copies of Nup93 and two copies of each Nup188 and Nup205. Two sets of two copies of Nup155 present in a head-to-tail manner and are in close proximity with 4 copies of Nup93. The Nup93 connects the CNT to the scaffold complex. The global resolution for this tomogram was 4.2 Å, and no biochemical interactions were reported in the paper (Huang et al., 2022).

A similar study conducted for Human NPC yielded an IR complex at a 12.6 Å resolution by using cryo-electron tomography and integrative structural modelling. From the reported PDB (7R5K), the C-terminal of the Nup93 was shown in close proximity with the C-terminal of Nup155 (Mosalaganti et al., 2022). A segmentation study was carried out in our lab for Nup155 and Nup93 in the complex, showing the segmentation for *H. sapiens*, *S. cerevasie* and *X. laevis* species (Figure 3). From the segmentation study also, the C-terminal of the Nup155 is in close proximity with the C-terminal of the Nup93 across all the three different species.

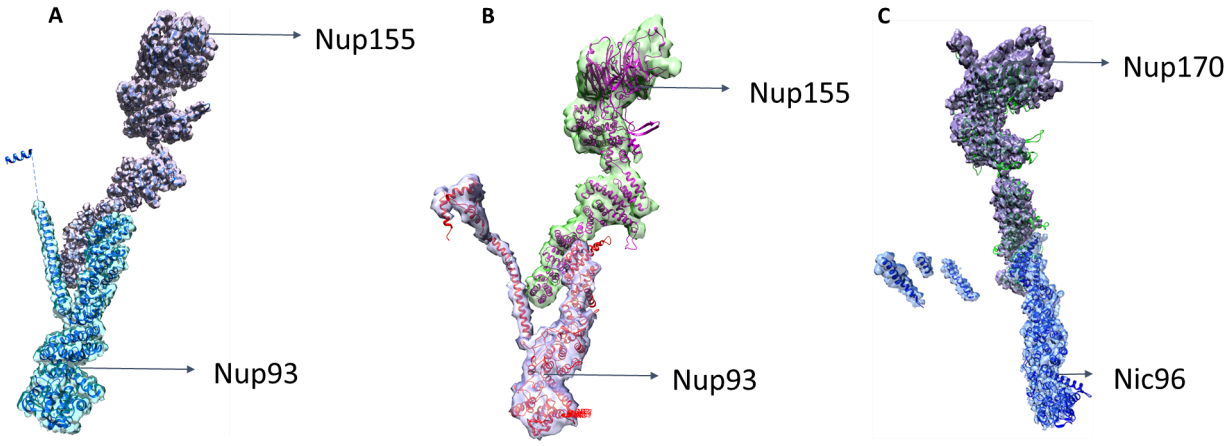

Figure 3. Segmentation maps of Nup155 and Nup93. (A) From *X. laevis* (B) From *H. sapiens* (C) From *S. cerevisiae*, Segmented in UCSF Chimera from *X. laevis*: EMD32566 with PDB7wkk; *H. sapiens*: EMD14322 with PDB7r5k; *S.cerevisiae*: EMD32658 with PDB7wot. (Credits: Megh)

The NPC structures captured and reported so far are in two states, either constricted or dilated. When the cargo crosses the selective barrier, the pore size increases from ~23 nm to ~37 nm in *X. laevis* (Eibauer et al., 2015). The same trend has been observed in humans also. For the human NPC, the IR diameter is found to be 54 Å in dilated, compared to a 42 Å in the constricted state. These studies were performed with cryo-focused ion beam specimen thinning (Mosalaganti et al., 2022). From cross-linking mass spectrometry data, it has been revealed that the Nup155 and Nup93 interacts each other via multiple interaction sites (Kosinski et al., 2016). This further suggests that Nup155 and Nup93 might be present in multiple conformations. To understand these conformational changes its very important to study them in cellulo. Given the complexities and the scale of interactions within the cell, conducting a comprehensive in vitro study of these complexes is essential to understand their various conformations.

1.5 Prediction of interaction interface of Nup155 and Nup93 using CoRNeA tool

CoRNeA (**Co**-evolution, **R**andom Forest, **Ne**twork **A**nalysis) is an in-silico prediction tool, which is trained on eukaryotic protein complexes, can predict protein-protein interaction interfaces between two given protein sequences (Chopra *et al.*, 2020). Between Nup93 and Nup155, it has predicted multiple interaction interfaces with some of them having very strong confidence score (region of $Nup93^{1-150}$ with $Nup155^{1-515}$) indicating strong interaction and some moderate in the region of $Nup93^{785-819}$ with $Nup155^{1-515}$ (Figure 4) (Sangeeta Niranjan et al., 2021). Also, In-vitro studies from the lab suggested that different regions of Nup155 interact with different regions of Nup93. From the previous work conducted in our lab, it has been shown that the N-terminal domain $Nup155^{1-515}$ interacts with $Nup93^{96-819}$, $Nup93^{176-819}$, $Nup93^{96-150}$, and with $Nup93^{1-150}$. But, this particular study focuses only on the interaction of **$Nup155^{1-515}$ with $Nup93^{599-819}$** and **$Nup155^{864-1391}$ with $Nup93^{1-819}$**. As from Figure 4, there is prediction that, there is an interaction between these domains.

S.No.	HsNup 93 amino acid residue	HsNup155 amino acid residue	Convolution Scores	No. of Pairs in the predicted region
1	96-107	286-289	267	44
2	96-106	138-142	198	41
3	536-546	127-131	165	40
4	785-792	138-142	162	36
5	800-810	286-289	152	32
6	800-809	952-958	124	31
7	86-93	1082-1088	114	30
8	99-105	55-59	112	29
9	96-106	1346-1348	106	28
10	371-378	120-122	102	22

Figure 4. Convolution score for different regions of *Hs*Nup93 and *Hs*Nup155. The dark blue colour shows high confidence of the interaction interface. Adapted from (Sangeeta Niranjan et al., 2021)

1.6 Rationale of the study

Inside the NPC, different nucleoporins interact among themselves to form the assembly. Adding to the complexity, the NPC rearranges its interaction patterns during constricted and dilated states. To get the correct picture of the whole NPC assembly, the structural characterization of the individual nucleoporin is important. With that, the information about the interacting partners of that nucleoporin as well as the characterisation of the interacting complex is also necessary. As mentioned above, to capture these complexes, one need to reconstitute them in-vitro. Also, from the CoRNeA based prediction, there are different interactions that exist in these nucleoporins. In the case of Nup155 and Nup93, different domains have a predicted interaction and in our lab it is well established that different domains of these proteins

interact with each other to make complexes. Due to their functional role in the cell, some interactions are stronger and some are transient. My aim for the project includes screening of these interactions and structurally characterising one such complex. It will give us better idea about confirmations of these complexes inside the cell.

1.7 Objectives of the thesis

In this thesis, I aim to carry out the standardisation of purification of Human Nup155 and Nup93 in the complex. The objective includes interaction studies of various domains of these proteins and screening the best combination to study the structure of complexes. The detailed list of objectives includes:

1) Interaction studies of $Nup155^{1-515}$.$Nup93^{599-819}$
2) Purification standardisation of $Nup155^{1-515}$.$Nup93^{599-819}$
3) Validation of interaction between $Nup155^{864-1391}$ and $Nup93^{1-819}$
4) Standardisation of $Nup155^{864-1391}$.$Nup93^{1-819}$ complex purification
5) Cryo-EM studies of $Nup155^{864-1391}$.$Nup93^{1-819}$

2. Material and methods

2.1 Transformation of plasmids in BL21 DE3 (RIL) cells

The competent BL21 DE3 (RIL) cells were thawed on ice for 20 minutes. 100-200 ng of the desired plasmid was added to the cells and incubated for 10 mins. Then, the cells were given a heat shock at 42°C for 90 seconds. Cells were kept on ice immediately after the heat shock for 10 minutes. After the incubation on ice, 500 µl of LB broth was added to the cells and incubated at 37°C for 1 hour witwerehaking. After the incubation, 10-20 µl of the total cells was plated on the agar plate containing appropriate antibiotics. The plates were incubated for 12-14 hours at 37°C.

For the primary culture, a single colony from the plate was added to the LB broth containing appropriate antibiotics. The inoculated culture was incubated for 12-14 hours overnight at 37°C with shaking.

For secondary culture, 1% of the primary culture (10 ml for 1 litre) was added to the LB broth containing appropriate antibiotics and incubated at 37°C till OD_{600} reached 0.6-0.8. After that, the cultures were incubated at 4°C for 30 minutes. Then, the IPTG was added to the culture at a final concentration of 0.4 mM. These cultures were then incubated at 18°C for the desired amount of time. Later, the cultures were pelleted down in a centrifuge at 4000 rpm for 15 mins. The pellets were washed with 1 x PBS pH 7.4 and kept at -20°C until further use.

2.1.1 For $Nup155^{1-515}$ and $Nup93^{599-819}$

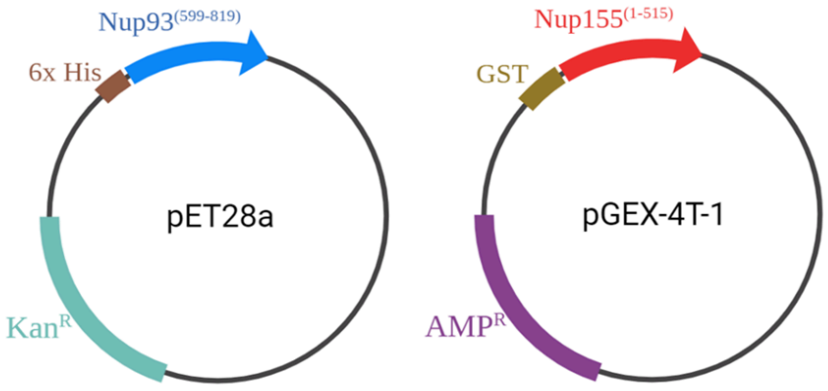

Figure 5. Constructs containing genes of $Nup93^{599-819}$ and $Nup155^{1-515}$. pET28a containing $Nup93^{599-819}$ and pGEX-4T-1 containing $Nup155^{1-515}$

The constructs were used for the transformation of the complex (Section 3.1). The size of Nup155$^{1-515}$ is ~84 kDa with a GST tag, and the size of Nup93$^{599-819}$ is ~26 kDa with a 6 x histidine tag (Figure 5).

2.1.2 For Nup155$^{864-1391}$ and Nup93$^{1-819}$

The constructs were used for the transformation of the complex (Section 3.2). The size of the Nup155$^{864-1391}$ with the 6 x histidine tag is ~60 kDa, and size of Nup93$^{1-819}$ is ~145 kDa, with N-terminal GST and C-terminal GFP tag (Figure 6).

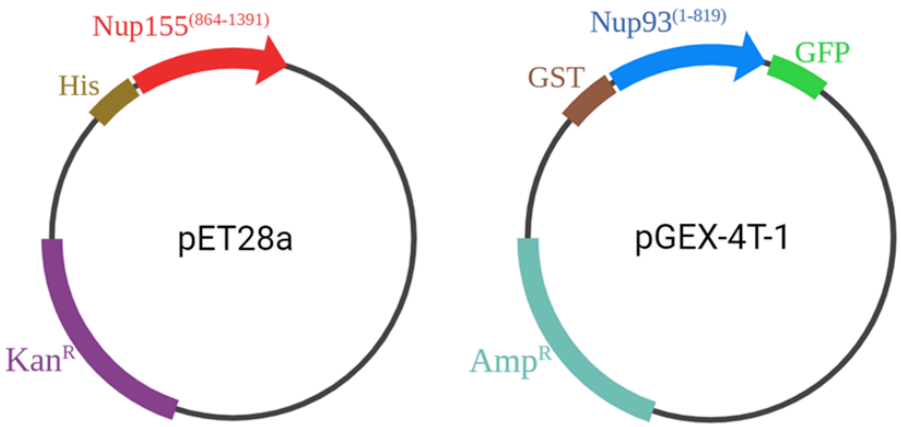

Figure 6. Constructs containing genes of Nup93$^{1-819}$ and Nup155$^{864-1391}$. pET28a containing Nup155$^{864-1391}$ and pGEX-4T-1 containing Nup93$^{1-819}$

2.2 Affinity purification

The pellets were thawed on the ice. The desired amount of lysis buffer (Table 1) was added to the pellet and resuspended by repeated pipetting. After the proper resuspension of the pellet, the pellets were sonicated at 35 Amp for 10 sec on and 10 sec off for a total pulse time of 2 minutes. The whole lysate was then centrifuged at 16,000 rpm for 50 minutes. The clear supernatant thus obtained was bound with glutathione agarose beads (Pierce) pre-equilibr30-column lysis buffer in an end-to-end rotor at 4°C for binding. The beads were washed with a 30 column volume (CV) of wash buffer (Table 1). Bound fractions were eluted with an elution buffer with 0.5 CV (Table 1). Similarly, for Ni-NTA purification, 1 ml Ni-NTA agarose beads were bound with elution

collected from GST affinity purification for 1 hour with Ni-NTA binding buffer. The beads were washed with a 30 CV of wash buffer. Bound fractions were eluted with an elution buffer of 0.5 CV (Table 2).

2.2.1 Co-mixing experiment for Nup155$^{1-515}$.Nup93$^{599-819}$ complex purification

The pGEX-4T-1 containing Nup155$^{1-515}$ and pET28a containing Nup93$^{599-819}$ were transformed individually into the BL21 DE3 (RIL) cells. A total of 5 litres of culture was grown: 4 litres for Nup155$^{1-515}$ and 1 litre for Nup93$^{599-819}$. Lysis buffer was added for the resuspension of the pellets, the resuspended pellets were mixed and subjected to homogenization. After that, the protein was purified with the GST affinity method.

2.2.2 Co-mixing experiment for Nup155$^{864-1391}$.Nup93$^{1-819}$ by GST affinity strategy

The pGEX-4T-1 containing Nup93$^{1-819}$ and pET28a containing Nup155$^{864-1391}$ were transformed individually into the BL21 DE3 (RIL) cells. 2 litres of Nup93$^{1-819}$ pellet was used with 0.25 litres of Nup155$^{864-1391}$. The resuspended pellets were mixed and later sonicated. The supernatant thus obtained was purified with the GST affinity method.

2.2.3 Purification of Nup155$^{864-1391}$.Nup93$^{1-819}$ by GST anti-GFP nanobody

The pellets were processed similarly as given in section 2.2 till obtaining the clear supernatant. 1 ml of glutathione agarose beads were first equilibrated with (20 mM Tris-Cl, 150 mM NaCl). Then 0.8 mg/ml GST tagged anti-GFP nanobody protein was bound with the equilibrated beads for 1 hour, as displayed in figure 7. After binding, the beads were incubated with the clear supernatant obtained from the pellets, further the beads were washed with wash buffer (Table 1), and the protein was eluted with the elution buffer (Table 1) containing 0.005% DDM.

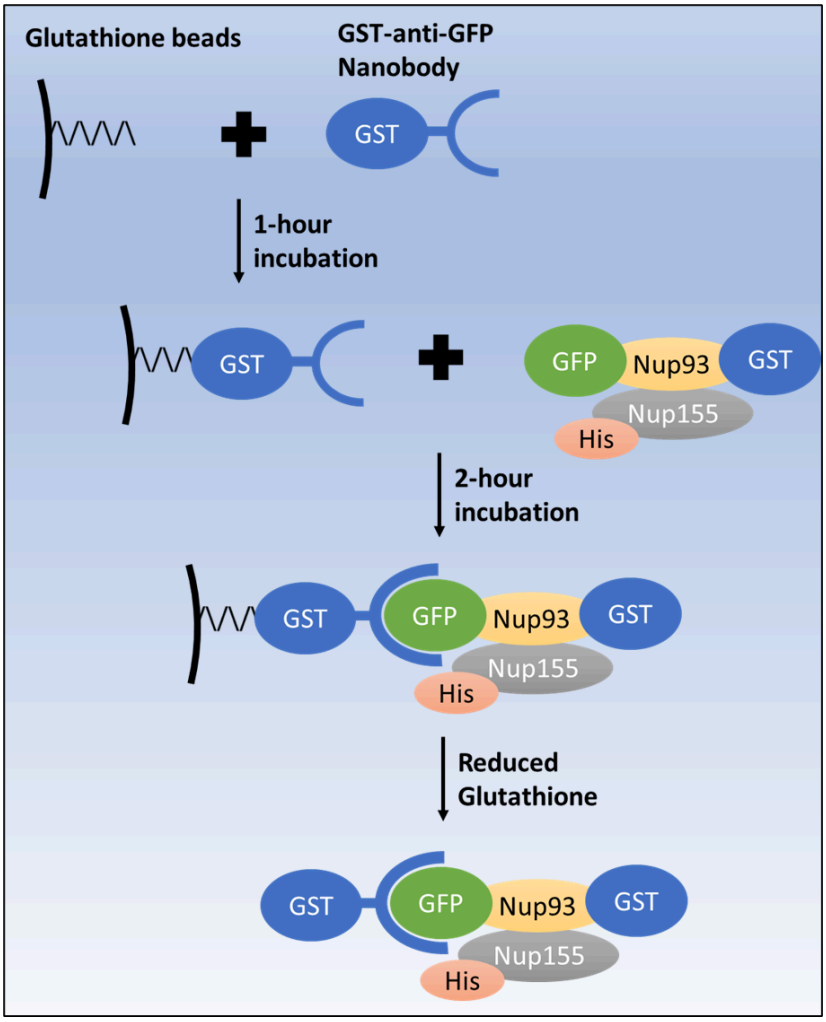

Figure 7. Purification strategy by GST tagged anti-GFP nanobody. Different steps in anti-GFP nanobody based purification.

2.3 Size exclusion chromatography

For size exclusion chromatography, two columns were used, including Superdex 200 Increase 10/300 GL (24 mL) and Superose 6 Increase 10/300 GL (24 mL). Firstly, the column was washed with 1 - 2 CV of Milliq. Later, the column was equilibrated by passing 1 CV of buffer with a flow rate of 0.3 ml/min. Once the column has been equilibrated, the samples were injected into the column. The volume corresponding to the molecular weight of the complex was collected and run on the SDS-PAGE gel. Simultaneously, the UV chromatogram has been plotted.

Table 1 GST lysis buffer composition

Sr. no.	Components	Lysis (mM)	Wash (mM)	Elution (mM)
1.	Tris-Cl pH 7.5 (1 M)	50 mM	50 mM	50 mM
2.	NaCl (5 M)	300 mM	300 mM	300 mM
3.	EDTA (0.5 M)	0.5 mM	0.5 mM	0.5 mM
4.	DTT (1 M)	1 mM	1 mM	-
5.	PMSF (0.2 M)	1 mM	-	1 mM
6.	Glycerol (50%)	5 %	2 %	2 %
7.	$MgCl_2$ (1 M)	2.5 mM	-	-
8.	DDM (10%)	1 %	0.5 %	0.25 %
9.	Red. glutathione	-	-	10 mM

Table 2 Ni-NTA binding buffer composition

Sr. no.	Components	Lysis (mM)	Wash (mM)	Elution (mM)
1.	Tris-Cl pH 7.5 (1 M)	50 mM	50 mM	50 mM
2.	NaCl (5 M)	300 mM	300 mM	300 mM
3.	β-Me (14.3 M)	5 mM	-	-
4.	PMSF (0.2 M)	1 mM	-	1 mM
5.	Glycerol (50 %)	2 %	-	5 %
6.	$MgCl_2$ (1 M)	2.5 mM	-	-
7.	DDM (10%)	0.25 %	0.25 %	0.25 %
8.	Imidazole (1 M)	-	40 mM	300 mM

2.3.1 Size exclusion chromatography for $Nup155^{1-515}$.$Nup93^{599-819}$

Biorad HPLC was used with Superdex 200 Increase 10/300 GL (24 ml) column with a flow rate 0.25 ml/min. 0.25 ml fractions were collected from the elution buffer (20 mM Tris-Cl pH 7.5, 300 mM NaCl, 0.5 mM EDTA, 2 mM DDM). The peak fractions were loaded on 12 % SDS-PAGE and stained with silver stain.

2.3.2 Size exclusion chromatography for $Nup155^{864-1391}$.$Nup93^{1-819}$

A) After GST affinity chromatography

AKTA HPLC system was used for the size exclusion chromatography and the Superdex 200 Increase 10/300 GL (24 ml) column with a flow rate of 0.3 ml/min. 0.25 ml fractions were collected from the elution buffer (20 mM Tris-Cl pH 7.5, 300 mM NaCl, 0.5 mM EDTA). The peak fractions were loaded on 12 % SDS-PAGE and stained with coomassie stain. In the unconcentrated injection, the protein concentration was 0.3 mg/ml and in the concentrated injection the concentration was 0.6 mg/ml.

B) After the on-bead thrombin digestion

After the washing step in the GST affinity, the glutathione beads were incubated with the thrombin for 12 hours at 4°C and eluted with elution buffer without glutathione. AKTA HPLC system was used for the size exclusion chromatography and the Superdex 200 Increase 10/300 GL (24 ml) column with a flow rate of 0.3 ml/min. 0.25 ml fractions were collected from the elution buffer (20 mM Tris-Cl pH 7.5, 300 mM NaCl, 0.5 mM EDTA). The peak fractions were loaded on 12 % SDS-PAGE and stained with coomassie stain.

C) Co-mixing experiment followed by SEC

The pGEX-4T-1 containing $Nup93^{1-819}$ and pET28a containing $Nup155^{864-1391}$ were transformed individually into the BL21 DE3 (RIL) cells. 2 litres of $Nup93^{1-819}$ pellet was used with 1 litre of $Nup155^{864-1391}$. The $Nup155^{864-1391}$ with a 6 x histidine tag, was purified with Ni-NTA affinity and $Nup93^{1-819}$ having a GST tag, was purified by GST affinity. For

unconcentrated injection, both the elutions were mixed in a vial and incubated on ice for 30 minutes. For the concentrated run, the proteins were mixed and kept on ice for 30 minutes. Later, the fractions were concentrated 4 times and injected on the Superdex 200 Increase 10/300 GL. The elutions were collected in the elution buffer (20 mM Tris-Cl pH 7.5, 300 mM NaCl, 0.5 mM EDTA).

D) GST affinity followed by SEC in the presence of DDM

AKTA HPLC system was used for the size exclusion chromatography and the Superdex 200 Increase 10/300 GL (24 ml) column with a 0.3 ml/min flow rate. 0.25 ml fractions were collected from the elution buffer (20 mM Tris-Cl pH 7.5, 300 mM NaCl, 0.5 mM EDTA, 0.005% DDM). The peak fractions were loaded on 12 % SDS-PAGE and stained with coomassie stain.

2.4 SDS-Polyacrylamide gel electrophoresis

The composition of the reagents were used from the Ridley, 1989. Firstly, the reagents were mixed for the resolving gel. Then stacking gel was prepared and poured above the resolving gel. The desired gel percentage was run by putting it in the tank with the Tris-glycine-SDS buffer. The samples were heated at 95°C for 5 minutes by adding loading dye (5% SDS, 100 mM β-mercaptoethanol, 250 mM Tris-Cl pH 6.8, 0.1% bromophenol blue, 50% Glycerol). The gel was run at 100 V till the dye front reached to the bottom. Then, the gel was stained in the coomassie dye (50% Methanol, 10% acetic acid) for 20-40 minutes and removed overnight in the destain (20% Methanol, 10% acetic acid). The gel was imaged, after complete destaining.

2.5 Western blotting

After the gel run was completed, as mentioned in Section 2.4, the gel was removed and placed over the PVDF (Polyvinylidene fluoride) membrane by closing the gel and the membrane in a cassette in the transfer buffer (Tris-glycine-SDS, 20% Methanol). The transfer was set for 2 hours at 75 V. After the successful transfer, the PVDF membrane was kept in the blocking solution (5 % skimmed milk) for 1 hour at room temperature. After blocking the membrane, the membrane was incubated with

either of the primary antibody: anti-his (Sigma #H1029), anti-GST (Sigma #G1160), anti-GFP (Sigma #G1546) and anti-GST HRP-conjugated (RPN1236V). The primary antibodies were prepared in 1 X PBST in a 1:3000 ratio. The membrane was then incubated with the primary antibody for 12-14 hours. Subsequently, on the next day, the primary antibody was removed, and the membrane was washed with 1 x PBST, 3 times for 10 minutes. Then, the membrane was incubated with the HRP-conjugated secondary mouse IgG (Sigma #A3673) at 1:5000 dilution and incubated at room temperature for 1 hour. Then, the secondary antibody was removed, and the membrane was washed three times with 1 x PBST for 10 minutes each. Images were recorded using AMERSHAM ImageQuant 800.

2.6 Buffer exchange of protein

For the buffer exchange, Amicon 0.5 ml centrifugal filter was used. The filter was equilibrated with the elution buffer. Then, the protein was added to the filter and spun at 2000 rcf for 1 minute each. After the run, the concentrated fraction was remixed with the protein sample and filled again with the protein. This procedure was used to reach the desired concentration of the protein.

2.7 Cross-linking experiments

For the cross-linking experiments, the cross-linker glutaraldehyde was used. 0.1%, 0.01% and 0.001% concentrations of glutaraldehyde were freshly prepared from 25 mg/ml stock in the elution buffer. These final concentrations were added with 45 µl of the protein (0.1 mg/ml), and the reaction was incubated for 10 mins. After 10 minutes, 1 M Tris-Cl pH 7.5 was added to the final concentration of 50 mM to quench the reaction. Two sets of these reactions were performed for undigested protein and thrombin-digested protein. These quenched reactions were loaded on 8% SDS-PAGE gel to verify the cross-linked protein.

2.8 Cryo-electron microscopy of protein

Firstly, grid preparation was performed for Au Flat 300 mesh Gold grid 1.2/1.3, in which 4 µl (0.19 mg/ml) of protein was loaded onto the grid. After that, those grids were screened with the screening microscope. The good grid squares were selected for the final data collection at 200 KeV by Talos Arctica G2 microscope. The defocus range was from -0.5 µm to -2.0 µm. A total of 3284 movies were collected from the grid at electron exposure of 40 / $Å^2$ with a pixel size of 1.2 Å.

2.9 Cryo-EM data processing

The software Cryosparc was used to solve the cryo-EM data. All the steps, like patch motion correction, Contrast Transfer Function estimation, particle picking, and 2D classification were performed using Cryosparc 4.3.1.

A Total of 3284 micrographs were subjected to patch motion correction, followed by patch CTF correction. From that, ~1400 micrographs were manually curated for the data processing. From these micrographs, firstly elongated shape protein was picked manually. The manually picked particles were extracted, and classified by using 2D classification tool. These classes were further used to pick the particles by the template-based picker. The particles were extracted with the help of box size of 480 pixels (1 px = 0.60 Å). These particles were screened and subjected for multiple rounds of 2D classification. Final round of 2D classification yielded 11,291 particles in 10 different classes.

3. Results

3.1 Purification standardisation of Nup155$^{1-515}$.Nup93$^{599-819}$

The 1-515 region of the protein Nup155 is a β-propeller, from the 5.2 Å Cryo-EM structure PDB (7EYF) (Sangeeta Niranjan et al., 2021). This region was already cloned with the N-terminal GST tag in the pGEX-4T-1 vector by Dr Sangeeta in our lab. Apart from being used as an affinity tag in chromatography, this fused tag increases the protein's solubility. Similarly, the C-terminal of the Nup93$^{599-819}$ which is a alpha-solenoid structure from PDB (7MW0) was already cloned in the pET28a vector with the N-terminal 6 x histidine tag by Dr Radha. The reason for having different tags for the proteins is to achieve high purity with the help of tandem affinity purification and also useful for the interaction studies. The following studies were performed as mentioned in methods (Section 2) and the Buffer conditions as given in (Table 1, 2).

3.1.1 Interaction of Nup155$^{1-515}$.Nup93$^{599-819}$

As predicted from the CoRNeA, there is a low convolution score between the N-terminal of the Nup155 and the C-terminal of the Nup93. To verify that, as mentioned

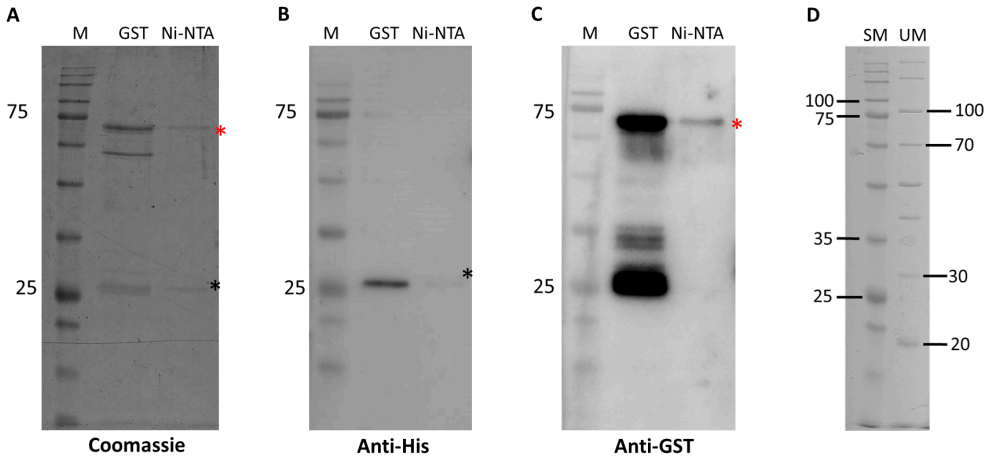

Figure 8. Confirmation of interaction for complex Nup155$^{1-515}$.Nup93$^{599-819}$. M - Marker (A) 12% SDS-PAGE gel stained with coomassie showing elution fractions loaded after GST and Ni-NTA affinity purification (B) blotted with anti-His antibody showing Nup93$^{599-819}$ (C) Anti-GST western blot analysis showing band for Nup155 in GST affinity, D) 12 % SDS-PAGE gel showing

mobility of stained marker (SM) and unstained marker (UM), band of Nup155 highlighted by '*' and Nup93 band highlighted by '*'.

in the Section 2.1, the proteins were purified with the GST affinity followed by Ni-NTA affinity. As in Figure 8 A, the two marked bands can be seen after the Ni-NTA affinity. This was later confirmed by the western blotting that the protein around 25 kDa was Nup93$^{599-819}$ with 6 x histidine tag, as it got detected by the anti-his antibody. Also, a band corresponding to ~75 kDa can be seen in the anti-GST western blot. These bands were again verified in the subsequent experiments. This experiment confirmed the formation of the complex in vitro.

3.1.2 SDS-PAGE gel profiles of Nup155$^{1-515}$ and Nup93$^{599-819}$

Since this is a protein complex, the individual profiles of the two proteins were checked after purification. Both the Nup155$^{1-515}$ alone and co-transformed Nup155$^{1-515}$.Nup93$^{599-819}$, were purified with GST affinity. Similarly, Nup93$^{599-819}$ having 6 x histidine tag, was purified with Ni-NTA affinity. Purified GST was also loaded to assess the corresponding GST band. Here, due to the similar molecular weight of the GST and Nup93$^{599-819}$ (~26 kDa) on the SDS-PAGE gel, a doublet band was detected. To confirm the bands of Nup93$^{599-819}$ and GST, western blotting was performed with 3 different samples: 1) with both the bands (Elution 1), 2) having the top band (Elution 6) and 3) having the lower band (Wash 3). By analysing the SDS-PAGE gel and the corresponding western blot, we concluded that the top band is the Nup93$^{599-819}$ having a histidine tag. This conclusion was drawn from the sample w3, as a band was detected in the anti-his blot and was absent in the anti-GST blot (Figure 9).

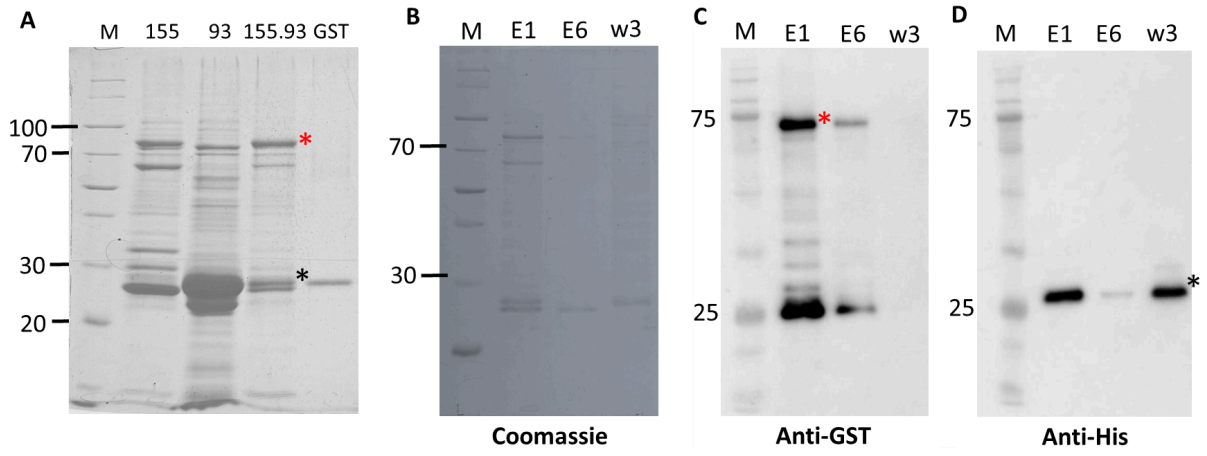

Figure 9. Analysis of proteins in the complex by SDS-PAGE and western blotting. M-marker (A) Showing (Only Nup155 with GST affinity, 93 (Only Nup93 with Ni-NTA affinity), 155.93 (155.93 complex by GST affinity), Purified GST. B,C,D) 12% SDS-PAGE, E1- Elution 1, E6 – Elution 6, w3 – 3rd wash, (B) Stained with Coomassie (C) blotted with anti-GST antibody (D) blotted with anti-his antibody, band of Nup155 highlighted by '*' and Nup93 band highlighted by '*'.

3.1.3 Standardisation of the parameters in purification

Here, 3 parameters were standardised to obtain best yield and stable complex.

A) Optimisation of bead binding incubation time

The bead binding time was optimised for this complex. Since, the first affinity purification strategy was decided as GST affinity, the following experiments were performed with only $Nup155^{1-515}$. After the sonication and high-speed centrifugation step, the supernatant was incubated with the 2 ml glutathione agarose beads for 2 hours, 4 hours and 8 hours time points. In the SDS-PAGE gel (Figure 10 A), even after 2 hours of bead binding incubation time, an adequate amount of protein is in the elutions from the corresponding band intensity. Hence, the 2 hours of binding time with the GST glutathione beads was optimised for the upcoming standardisation.

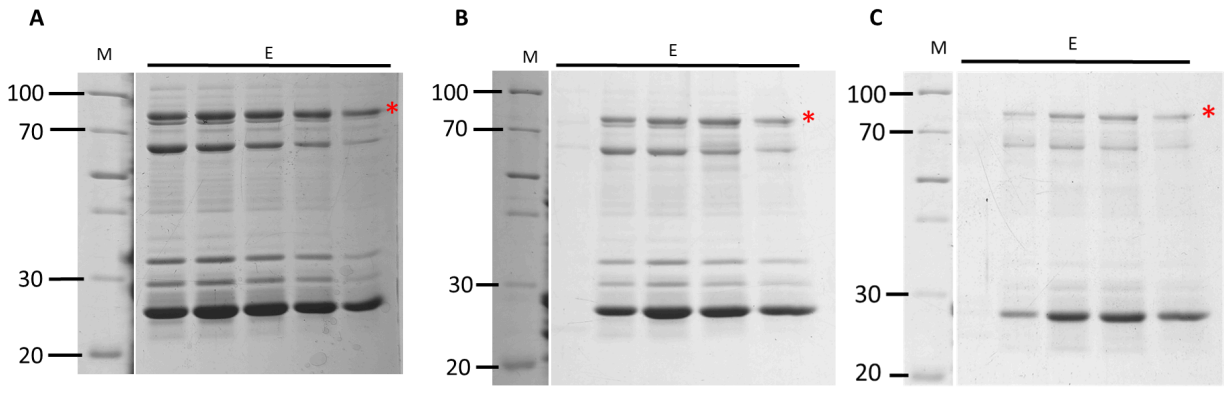

Figure 10. Standardisation of bead binding incubation time. M– Marker, E– Elutions, 12% SDS-PAGE (A) The supernatant incubated with beads for 2 hours rotating, (B) for 4 hours, (C) for 8 hours, band of Nup155 highlighted by '*'.

B) Optimisation of post-induction incubation time

Secondly, the post-incubation time after induction was optimised with the co-transformed pellets. After the induction step (Section 2.1), the induced cultures were incubated for 4 hours, 8 hours and 16 hours and pelleted afterwards.

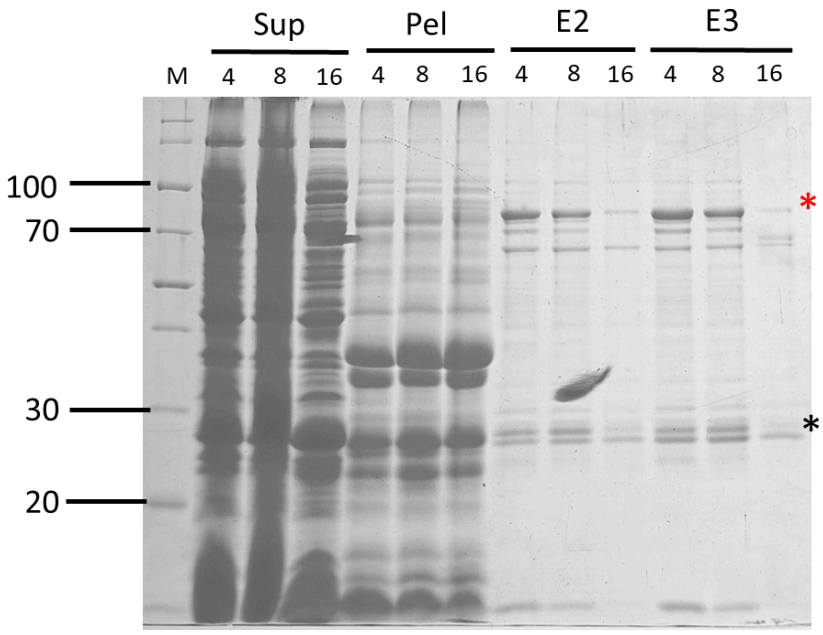

Figure 11. Standardisation of post-induction incubation time. M- Marker, Sup- Supernatant, Pel- Pellet, E - Elution, 12% SDS-PAGE gel , 4,8,16- time in hours post-induction, the band of Nup155 highlighted by '*' and Nup93 band highlighted by '*'.

Following that, GST affinity chromatography was performed on each of the 1-litre pellets. And the elutions were loaded on the 12% SDS-PAGE gel. From the band intensity, it was clear that the relative protein concentration of $Nup155^{1-515}$ was more for the 4 hours time point in both Elution 2 and 3 fractions (Figure 11). Since the supernatant fractions show that the net protein in the supernatant for the 16 hours time point is less, the protein might have eluted less in the elutions (Figure 11, Lane Sup16 and E2 16). Also, since we knew that the upper band in the lower doublet band is $Nup93^{599-819}$ (Section 3.1.2), the band intensity of 16 hours was less compared to 4 hours post induction time point in the E2 fraction. We concluded that the 4 hours post-induction incubation time is the best compared to 8 hours and 16 hours. This standardised condition was again verified with further experiments (Section 3.1.5).

C) Optimisation of lysis buffer volume

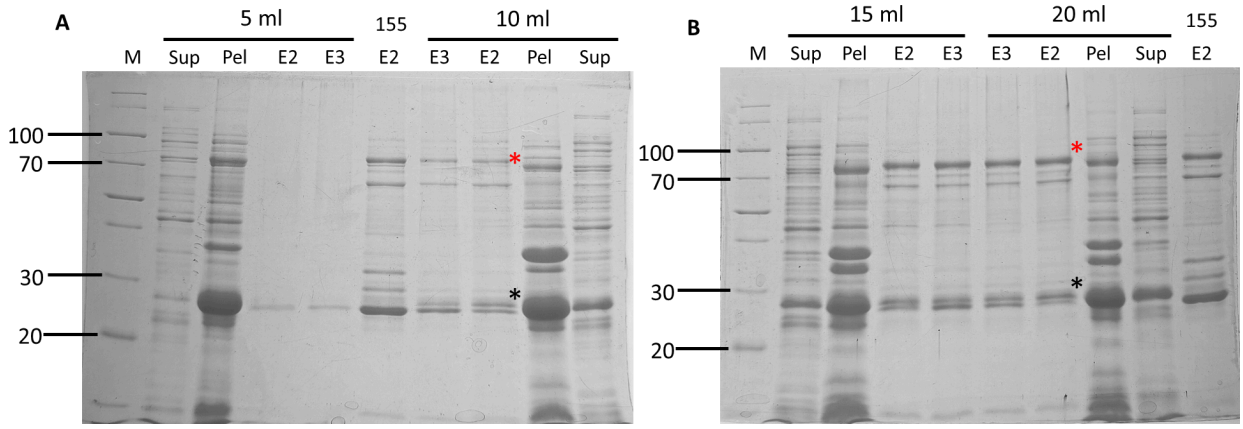

Figure 12. Standardisation of lysis buffer volume. M- Marker, E (2,3)- Elutions, Sup- Supernatant, Pel- pellet, 12% SDS-PAGE gel (A) Lysis buffer volume 5 ml and 10 ml, (B) Lysis buffer volume 15 ml and 20 ml, band of Nup155 highlighted by '*' and Nup93 band highlighted by '*'.

Lastly, the lysis buffer volume was optimised for 1-litre pellet for conditions by 5 ml, 10 ml, 15 ml and 20 ml. In the 15 ml and 20 ml of lysis buffer volume, the band intensity was higher than the 5 ml and 10 ml. Hence, 15 ml of lysis buffer was finalised for the further purification.

From the above results, the optimised conditions for the upcoming experiments were the following:

Condition	Post Induction time	GST binding time	Lysis Buffer Volume
1.	**4 hours**	**2 hours**	5 ml
2.	8 hours	4 hours	10 ml
3.	16 hours	8 hours	**15 ml**
4.	-	-	20 ml

Construct	155 Alone	155 + 93 Complex	Optimised Condition

Table 3. Optimised conditions for purification of Nup155$^{1-515}$.Nup93$^{599-819}$

3.1.4 Co-mixing strategy to increase yield

Here, we used the co-lysing strategy to increase the protein yield and to examine the possibility of complex formation (Section 2.2.1). Since the expression of the Nup93$^{599-819}$ was more compared with the Nup155$^{1-515}$. The pellets containing proteins: 4 litres of Nup155$^{1-515}$ and 1 litre of Nup93$^{599-819}$ were co-lysed with sonication and purified using GST affinity. The outcome indicates the absence of Nup93$^{599-819}$ on the SDS-PAGE gel (Figure 13 A). In subsequent western blot analysis, the Nup93$^{599-819}$ failed to get detected in the elution of co-lysed fractions, and was detected in the co-transformed and in only Nup93$^{599-819}$ frraction (Figure 13 B). This confirmed that the complex formation was unfeasible by using co-mixing strategy.

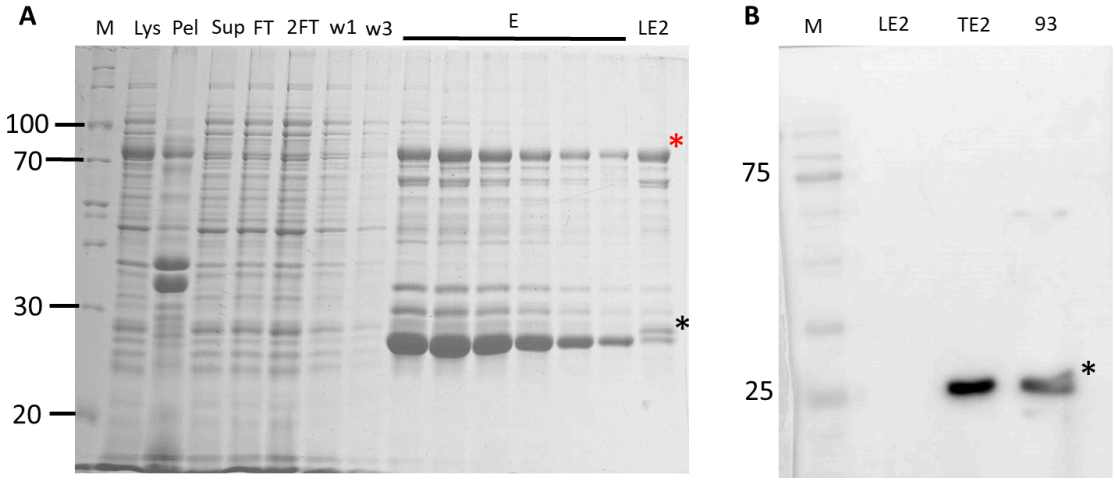

Figure 13. Co-mixing experiment of Nup155$^{1-515}$.Nup93$^{599-819}$. M- Marker, E- Elutions, Sup- Supernatant, Pel- pellet (A) 12% SDS-PAGE gel after GST affinity of co-lysed pellets, (B) Western blot analysis, blotted with anti-his antibody of co-lysed (LE2) and co-transformed (TE2) and Nup93 (93) purified by Ni-NTA as a positive control, elution bands of Nup155 highlighted by '*' and Nup93 band highlighted by '*'.

3.1.5 Optimisation of the yield of the complex Nup155$^{1-515}$.Nup93$^{599-819}$

With the above standardised conditions the culture volume was scaled up to 4 litres and purified with GST affinity. The purification was repeated multiple times for validation. The purification was performed with 4 litres and with varying the amount of the glutathione agarose beads of 2 ml and 4 ml (Figure 14 A, B). However, no significant improvement of band intensity was detected.

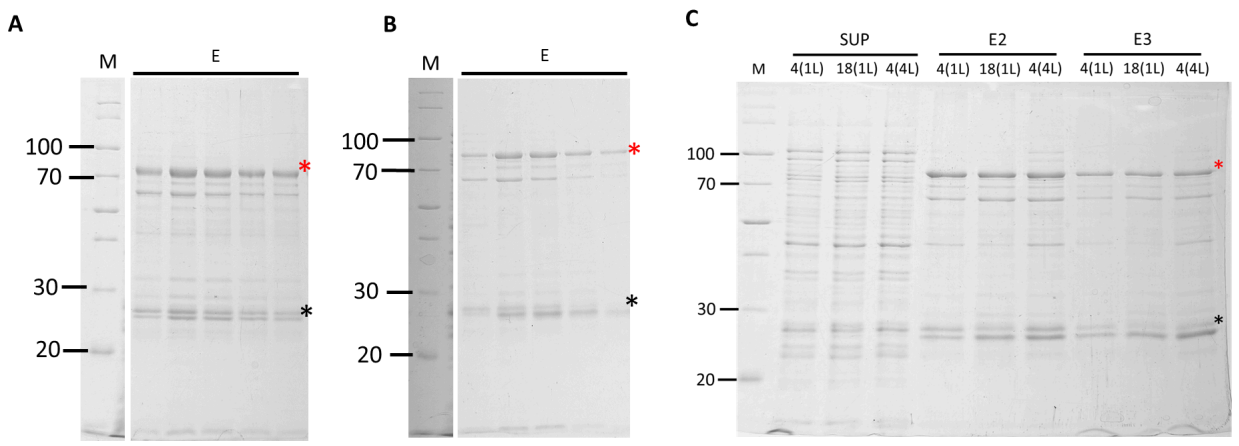

Figure 14. Affinity chromatography from 4 Litre culture volume. M- Marker, E- Elutions, Sup- Supernatant, Pel- pellet (A) GST affinity with 2 ml of glutathione beads, (B) GST affinity with 4 ml of glutathione beads (C) 4, 18: post-induction incubation time in hours, (1L) & (4L) Culture volume, elution bands of Nup155 highlighted by '*' and Nup93 band highlighted by '*'.

This was again verified in a single purification by comparing the profiles of 1 Litre and 4 Litre culture volume by using 2 ml beads. The band intensity Nup93$^{599-819}$ was more in 4 Litre compared to 1 Litre, in Elution 2 fraction (Figure 14 C). This verified the result discussed in (Section 3.1.3 B). The band intensity of the 1 Litre and 4 Litre was almost the same for Nup155$^{1-515}$. The result indicates that the yield of the complex cannot be improved by increasing the culture volume.

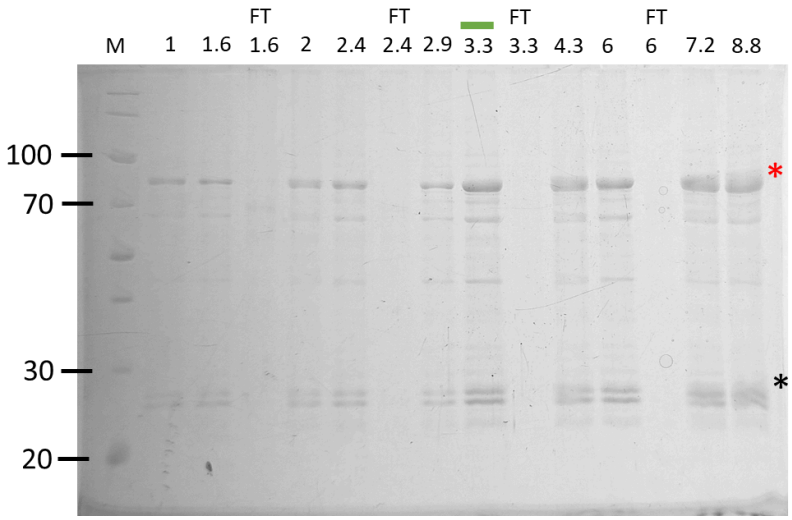

Figure 15. Standardisation of buffer exchange for Nup155$^{1-515}$.Nup93$^{599-819}$. M- Marker, FT- Flowthrough sample, Number represents times the volume was concentrated, bands of Nup155 highlighted by '*' and Nup93 band highlighted by '*'.

To solve the above-mentioned problem, we tried concentrating the protein with the help of a concentrator of 50 kDa. And found that the protein was concentrating up to 3.3 times the initial volume.

3.1.6 Size exclusion chromatography of Nup155$^{1-515}$.Nup93$^{599-819}$

Using the above standardised procedure for concentrating the protein, the protein was concentrated and loaded on the Superdex 200 Increase 10/300 GL (24 ml) column for the size exclusion chromatography. Different peak fractions were loaded on SDS-PAGE gel to validate the stability of the complex (Figure 16 A, B). In the gel, the fraction corresponding to 12.25 ml (where ~ 160 kDa molecular weight proteins elutes) has two bands corresponds to 25 kDa and 70 kDa. But in the western blot, it was detected that the lower band was in fact GST and not Nup93$^{599-819}$ as it failed to get detected by anti-his antibody. This concluded that post size exclusion chromatography, the complex was unstable and disintegrated.

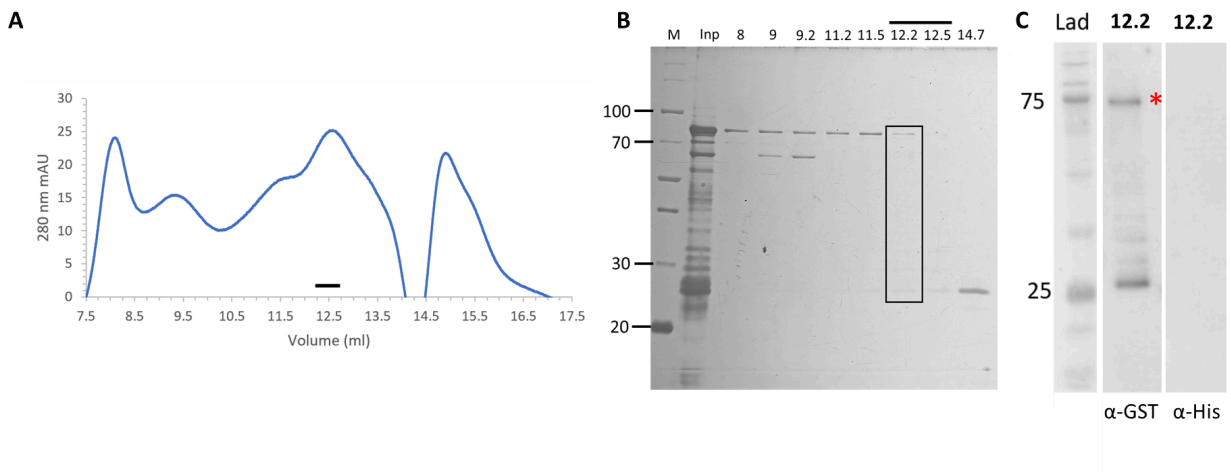

Figure 16. Size exclusion chromatography for the Nup155$^{1-515}$.Nup93$^{599-819}$. (A) Size exclusion chromatogram showing the peak regions and the corresponding volume in ml (B) 12% SDS-PAGE gel, stained with silver staining, M- Marker, numbers represents the elution volume of the Size exclusion column (C) Western blot showing anti-GST and anti-his blots for the 12.2 ml fraction, band of Nup155 highlighted by '*'.

3.2 Purification standardisation of Nup155$^{864-1391}$.Nup93$^{1-819}$

Similar studies were conducted on Nup93 full length having N-terminal GST and C-terminal GFP and Nup155 from 864-1391 with histidine tag. Also, both of the genes present in different vectors have different antibiotic selection markers (Section 2.1.2) so that various strategies can be used for purification.

3.2.1 Validation of interaction of Nup155$^{864-1391}$.Nup93$^{1-819}$

The following interaction studies were performed as mentioned in methods (Section 2). Buffer conditions for the affinity chromatography purification used as given in (Table 1, 2), without DDM detergent.

A) By GST affinity method

The theoretical molecular weight by adding the protein tags is ~145 kDa for Nup93$^{1-819}$, and ~60 kDa for Nup155$^{864-1391}$. To verify whether the Nup155$^{864-1391}$ and the Nup93$^{1-819}$ interact or not, both were co-transformed and purified by using GST affinity chromatography. Since, only Nup93$^{1-819}$ has a GST tag, it is expected that the

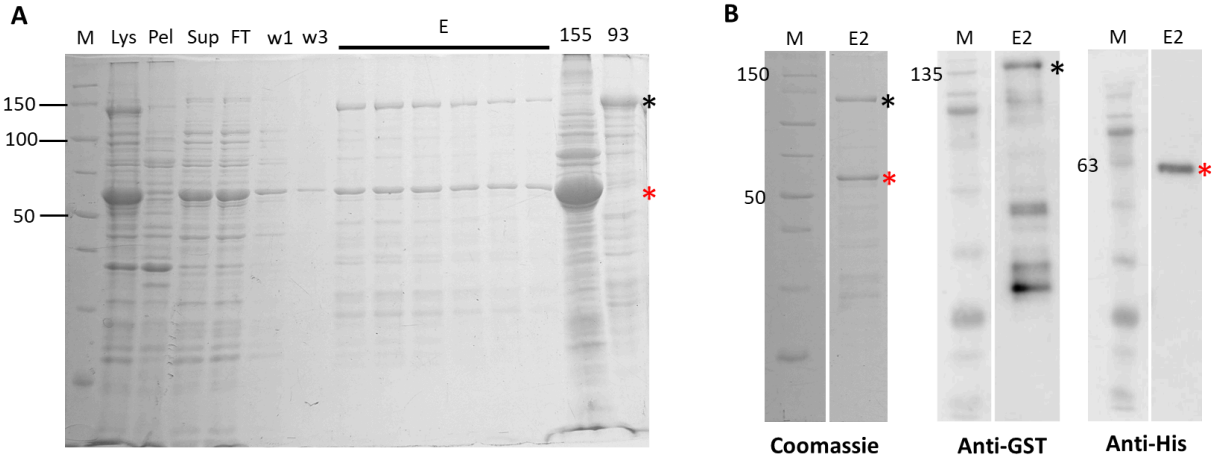

Figure 17. GST Affinity showing Nup155$^{864-1391}$ and Nup93$^{1-819}$ in the complex. M- Marker, E- Elutions, Sup- Supernatant, Pel- pellet, w- washes, 12 % SDS-PAGE gel (A) GST affinity with 2 ml of glutathione beads. The alone 155 was purified with the Ni-NTA affinity and 93 with GST affinity, loaded on the SDS-PAGE (B) Western blot analysis of Elution fraction 2, showing with the Coomassie, blotted with anti-GST, blotted with anti-His (From left to right), elution bands of Nup155 highlighted by '*' and Nup93 band highlighted by '*'.

interacting protein will co-elute with the Nup93$^{1-819}$, if the other protein is interacting with it. In SDS-PAGE gel, two prominent bands were detected, one close to 150 kDa and other greater than 50 kDa (Figure 17 A). Both the bands were approximately closer to the expected band size. To confirm the anticipated band position on the SDS-PAGE gel, the purified proteins were loaded onto the gel. Subsequently, the bands observed in the elutions were precisely aligned to the purified proteins. This concludes the presence of Nup155$^{864-1391}$ in the elution fractions, which confirms the interaction of Nup155$^{864-1391}$ with Nup93$^{1-819}$. For further confirmation, the second elution fraction of purified protein was blotted against anti-GST and anti-his antibody. For the anti-GST, a top band corresponding near 150 kDa was visible, and for the anti-his antibody, a band below 63 kDa was visible, confirming the presence of the 6 x histidine-tagged Nup155$^{864-1391}$.

B) By Ni-NTA affinity method

The GST affinity purified protein was then pooled, bound with the Ni-NTA beads, and purified further, as given in the methodology (Section 2.2). The appearance of both protein bands in Elution 2, 3, and 4 fractions confirmed the complex formation after tandem affinity chromatography (Figure 18).

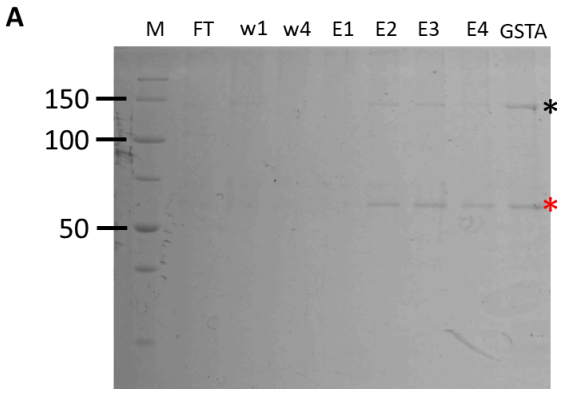

Figure 18. Purification with Ni-NTA affinity showing Nup155$^{864-1391}$.Nup93$^{1-819}$ in the complex. M- Marker, FT- Flowthrough, w- washes, E- elutions, GSTA- elution after GST affinity, 12% SDS-PAGE gel. Elution band lanes of Nup155 are highlighted by '*' and the Nup93 band highlighted by '*'.

C) By Size exclusion chromatography

To verify whether the complex was stable after size exclusion chromatography, the GST affinity purified protein fraction was injected into the Superdex 200 Increase 10/300 GL (24 ml) column as given in the methodology (Section 2.3.2 A). The visibility of a faint band in the elution was further confirmed with the anti-his western blotting, confirming the existence of Nup155$^{864-1391}$ and, ultimately, the complex in the elution. The complex was eluted at 9.5 ml in the concentrated sample, separated from the void peak at 8 ml. From the chromatogram for the standards, the >440 kDa proteins elutes at 9.5 ml on the Superdex 200 Increase 10/300 GL (24 ml) column. Since the Nup93$^{1-819}$ has a GST tag, the dimerisation of the fused protein might occur. This could be the reason for observing the complex being eluted at a higher molecular weight.

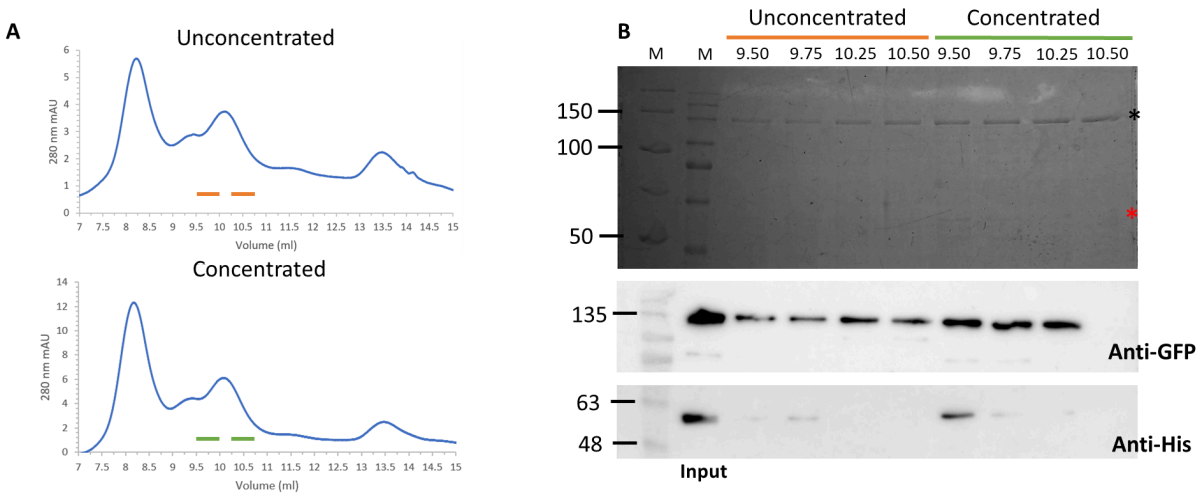

Figure 19. Confirmation after size exclusion chromatography for Nup155$^{864-1391}$.Nup93$^{1-819}$ purified with GST affinity. M- Marker, Corresponding volume in ml, Unconcentrated showing in (-) and concentrated showing in (-). 12% SDS-PAGE gel (A) Showing chromatogram of the size exclusion performed with Superdex 200 Increased 10/300 GL column (B) Gel showing size exclusion chromatography after GST affinity loaded with different volume, below corresponding western blot, blotted with anti-GFP and anti-his antibody, elution bands of Nup155 highlighted by '*' and Nup93 band highlighted by '*'.

D) GST tag digestion followed by size exclusion chromatography

Since GST is expected to form a dimer, in order to verify the presence of the complex in the absence of GST, the GST was digested overnight by adding thrombin as given in the methodology (Section 2.3.2 B). The GST digested fractions were injected into the Superdex 200 Increase 10/300 GL (24 ml). The chromatogram below had a shoulder peak corresponding from 10.6 ml to 12.4 ml, having the complex of interest. From the chromatogram for the standards, the ~150 kDa proteins elute at ~12 ml. After GST digestion, a clear shift was detected from 9.5 ml to 12 ml. This was further verified by using SDS-PAGE gel, the presence of two proteins was detected. This confirmed that the tag does not interfere with the complex formation.

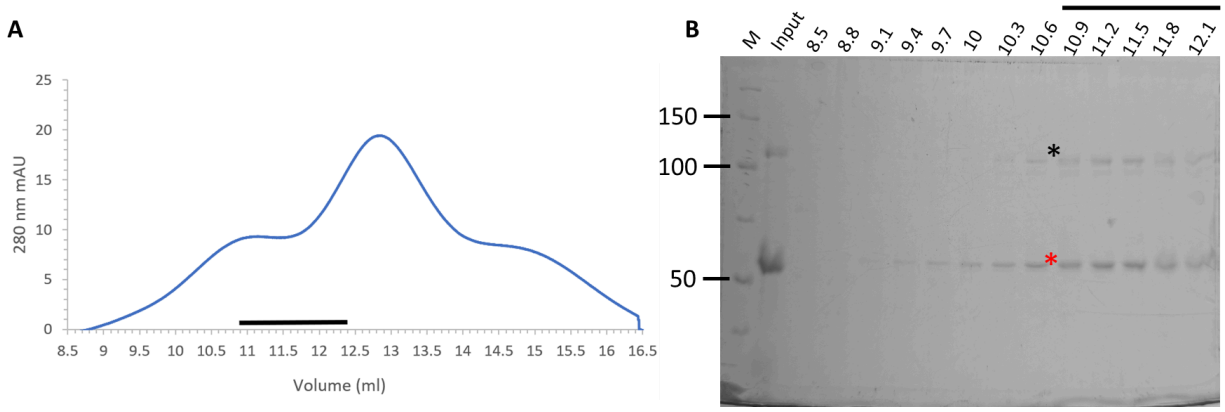

Figure 20. Size exclusion chromatography for Nup155$^{864-1391}$.Nup93$^{1-819}$ after on-bead thrombin digestion. (A) Size exclusion chromatogram showing the shoulder peak corresponding to the protein of interest (black line) (B) 10% SDS-PAGE gel showing the corresponding fractions, elution bands of Nup155 highlighted by '*' and Nup93 band highlighted by '*'.

E) By Co-mixing

E.1) Co-mixing purified proteins

Since the individual expression of proteins was higher than that of the co-transformed one (Figure 21 C). We tried a co-mixing strategy to inspect whether there was any improvement in the yield of the complex obtained. For this, Nup155$^{864-1391}$ with a 6 x histidine tag was purified with Ni-NTA affinity and Nup93$^{1-819}$ having a GST tag, was purified by GST affinity. The elution fractions of these purified proteins were

mixed and kept on ice for 30 minutes before injecting them into the Superdex 200 Increase 10/300 GL column (section 2.3.2 D). The fraction corresponding to 9.5 ml in the concentrated lane showed 1:1 stoichiometry from SDS-PAGE band intensity (Figure 21 B). This validated the formation of the complex via co-mixing.

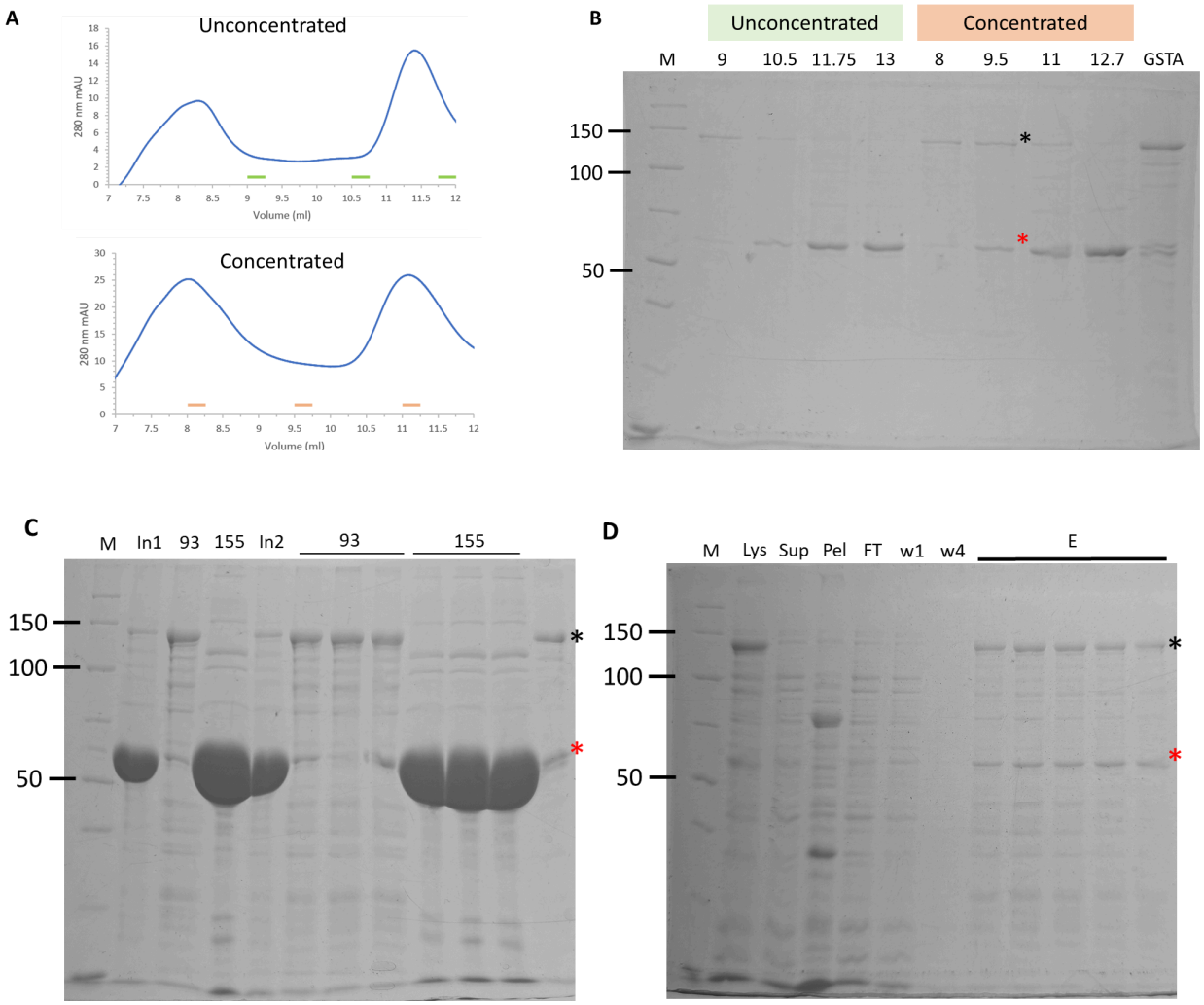

Figure 21. Purification of the complex by co-mixing. M- Marker, E- Elutions, Sup- Supernatant, Pel- pellet, w- washes, 10% SDS-PAGE gel (A) SEC chromatogram showing for the unconcentrated fraction (upper panel) and concentrated fractions (lower panel) (B) 10% SDS-PAGE gel showing the highlighted fractions loaded (green-Unconcentrated) and (red-concentrated), (C) In1/2 – the input injected on the SEC column, 93 & 155 are the purified proteins (D) 10% SDS-PAGE gel showing co-mixing pellets followed by GST affinity, elution bands of Nup155 highlighted by '*' and Nup93 band highlighted by '*'.

E.2) Co-lysing of pellets

The Nup155$^{864-1391}$ and Nup93$^{1-819}$ were transformed into BL21 DE3 (RIL) individually and pelleted separately. The pellets were lysed and purified with GST affinity (Section 2.2.2). In the elutions, the presence of both proteins was confirmed (Figure 21 D). Since only Nup93$^{1-819}$ has a GST tag, Nup93$^{1-819}$ pulled Nup155$^{864-1391}$. Hence, the formation of the complex was confirmed by GST affinity. This was also validated by size exclusion chromatography (3.2.1 E.1)

3.2.2 Buffer optimisation for Nup155$^{864-1391}$.Nup93$^{1-819}$

A) Use of DDM in the lysis and elution buffer

During the above experiments, the presence of a soluble, white, slimy precipitate was observed in the supernatant after the high-speed centrifugation step. This contamination was present even after the filtration through 0.45 µm filter and centrifugation. Further in analysis, we found out that the contamination was protein-specific. Similar contamination was observed in all the purifications containing the protein Nup155$^{864-1391}$. We concluded that the overexpression of Nup155$^{864-1391}$ contributed to the formation of soluble aggregates in the supernatant. The presence of any solubilising agent, such as detergent, can prevent aggregation. Hence we tried to use DDM in further purifications.

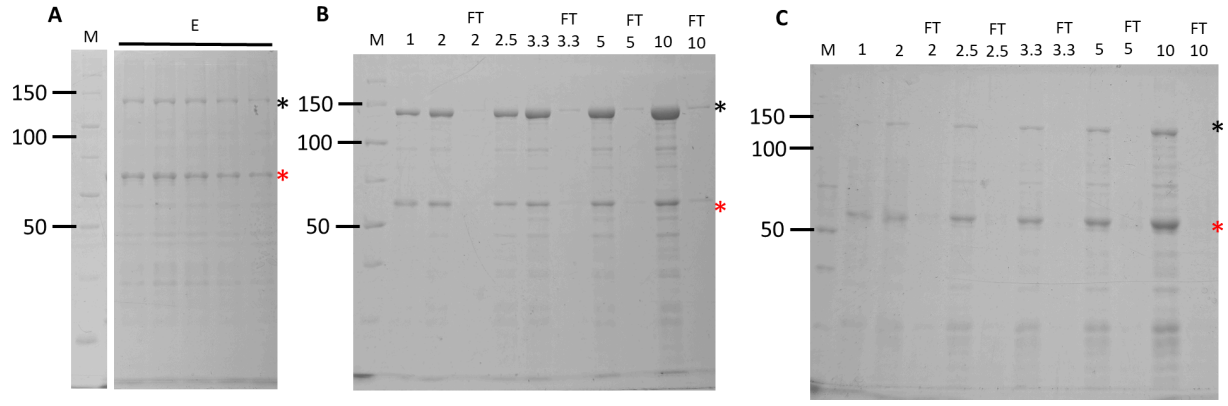

Figure 22. Standardisation of buffer exchange for Nup155$^{864-1391}$.Nup93$^{1-819}$ with DDM. M- Protein marker, E- Elutions, Sup- Supernatant, Pel- pellet, w- washes (A) GST affinity with 2 ml glutathione beads by using DDM throughout the purification. (B) 10% SDS-PAGE gel showing buffer exchange standardisation. The number represents that how many times the protein was

concentrated with respect to the initial volume. (C) 10% SDS-PAGE gel showing buffer exchange standardisation in the presence of 0.1mM DDM in the elution buffer. elution bands of Nup155 highlighted by '*' and Nup93 band highlighted by '*'.

DDM is a non-anionic detergent, stabilises the hydrophobic patches on the protein surfaces by surrounding them. Since in the previous purification, the band intensity of the Nup155$^{864-1391}$ was observed less, and got even fainter after size exclusion chromatography (Figure 19 B). Considering the aforementioned, we tried changing the buffer conditions by adding DDM throughout the purification. We added 1% in the lysis buffer, 0.5% in the wash buffer and 0.25% in the elution buffer. After GST affinity the band intensity of Nup155$^{864-1391}$ was equal to Nup93$^{1-819}$ (Figure 22 A). Later in the subsequent purification, the amount of DDM was further reduced to 0.005% in the elution. The buffer exchange optimisation was performed for both without DDM and with DDM purifications. Without DDM, the Nup155$^{864-1391}$ was concentrating less compared to Nup93$^{1-819}$ (Figure 22 B). However, even with the 0.005% DDM, the Nup155$^{864-1391}$ was concentrated (Figure 22 C). The observation can be due to the following reasons: first, since we have used 100 kDa centricon in both cases, in the absence of DDM, due to instability, the Nup155$^{864-1391}$ was precipitating and was not present in the soluble fraction. But in the other case where DDM is used, Nup155$^{864-1391}$ remained in the soluble fraction and concentrated with the Nup93$^{1-819}$.

B) Purification by GST tagged anti-GFP nanobody

Since the use of DDM enhanced the stability of the complex, we checked whether the purity and the yield of the protein complex could be improved further. As discussed earlier, the Nup93$^{1-819}$ also has a C-terminal GFP tag. The GST anti-GFP nanobody based purification was performed as given in the methods (Section 2.2.3). From SDS-PAGE gel band intensity, it clearly showed that the amount of protein was not enhanced by the GST anti-GFP nanobody based purification (Figure 23 A, B). The size exclusion chromatography was performed for the GST affinity purified elutions. In the chromatogram, a clear peak was observed from 10.9 ml to 13.6 ml on the Superose 6 Increase column (24 ml). The corresponding SDS-PAGE gel showed that the protein complex was present 1:1 from the band intensity. However, the band intensity of the Nup155$^{864-1391}$ was improved, as can be seen on SDS-PAGE gel stained with

coomassie, compared to the previous size exclusion chromatography without DDM (Figure 19 B).

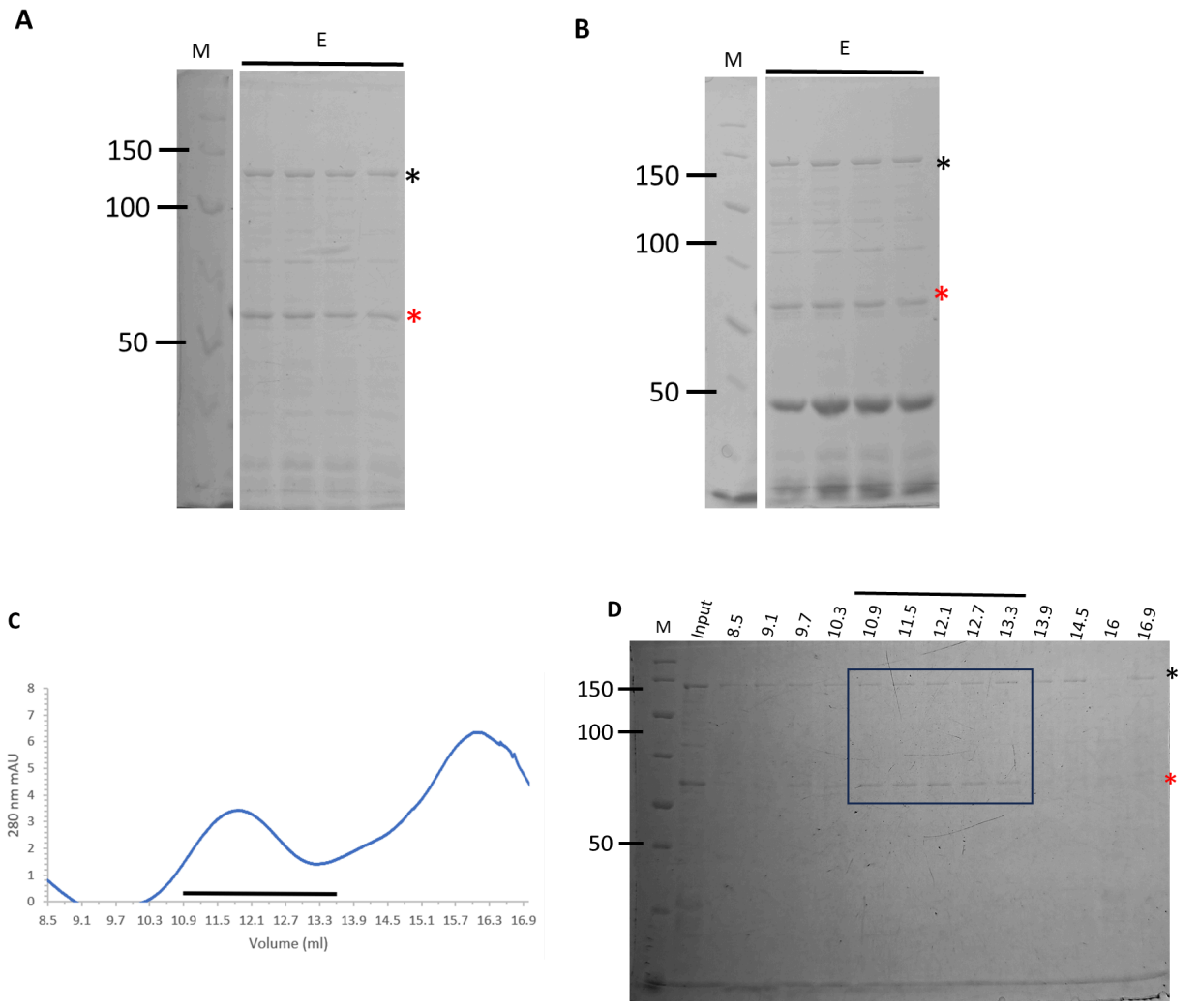

Figure 23. Affinity purification using GST tagged anti-GFP nanobody. M- Protein marker, E- Elutions (A) 10% SDS-PAGE gel showing GST affinity with 2 ml of glutathione beads using DDM throughout the purification. (B) 10% SDS-PAGE gel showing GST anti-GFP nanobody-based purification. (C) SEC chromatogram after GST affinity (D) 10% SDS-PAGE gel showing size exclusion chromatography for the GST affinity elutions. The fraction of interest is highlighted in the blue box. showing elution bands of Nup155 highlighted by '*' and Nup93 band highlighted by '*'.

C) Stability check for protein complex

GST affinity chromatography was performed on the fresh pellets for the stability check. A single fraction was concentrated up to 10 times, aliquoted in the vials and stored at different temperatures for the stability check. The protein was found stable at room temperature, 4°C, -20°C and after flash freezing (Figure 24 A).

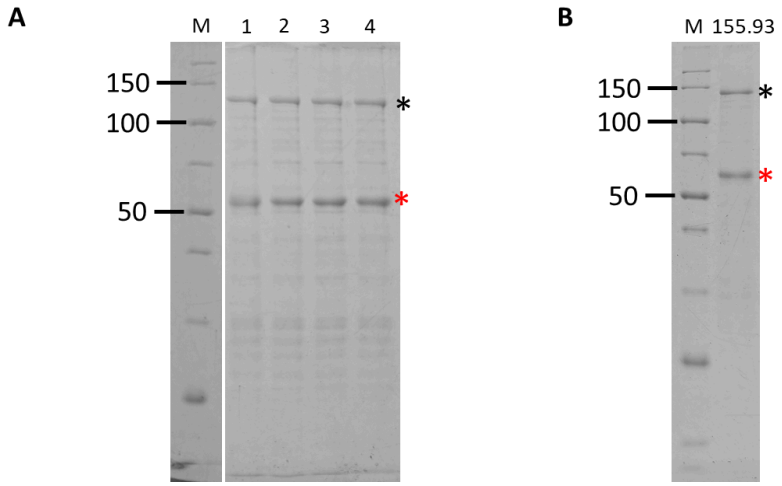

Figure 24. Stability check for the protein complex. M- Protein marker, (A) 10% SDS-PAGE gel showing protein stored at different temperatures, 1- Room temperature, 2- 4°C, 3- -20°C, 4- Flash froze (B) 12% SDS-PAGE gel showing the final protein used for cryo-EM. elution bands of Nup155 highlighted by '*' and Nup93 band highlighted by '*'.

D) Cross-linking of the complex

The cross-linking attempts were performed as mentioned in the methods (Section 2.7). The complex was cross-linked for 0.1% of the cross-linker. Also, the 10 minutes time was sufficient for the reaction to occur. The reactions with cross-linking with 0.1% glutaraldehyde and no digestion, thrombin digestion followed by 0.1% crosslinking and first 0.1% cross-linking and later digestion seemed to work as the band shifted above in these lanes (Figure 25). But these shifted bands does not corresponds with the expected molecular weight, suggesting formation of an aggregate. This need to be further standardised.

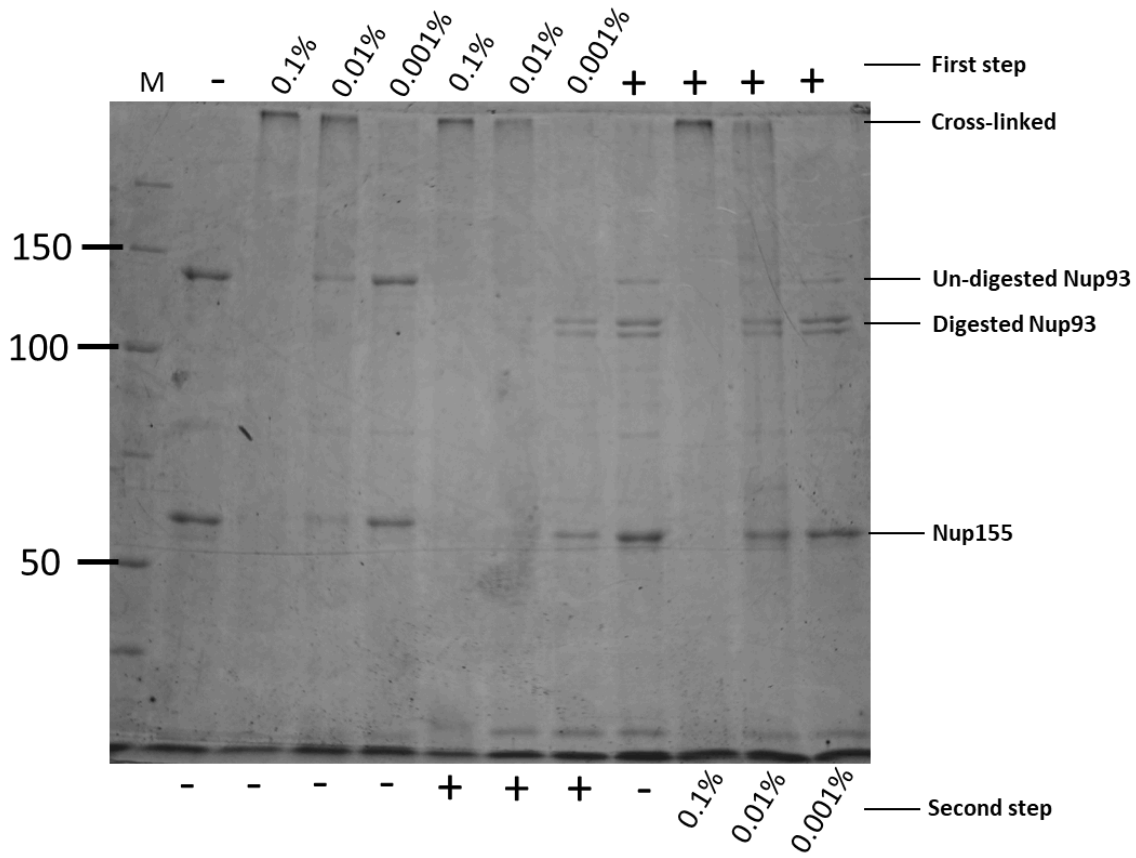

Figure 25. Cross-linking assay for the Nup155$^{864\text{-}1391}$.Nup93$^{1\text{-}819}$. 8 % SDS-PAGE gel, the top of the gel showing the first step in the assay, percentage of the cross-linker used. '+' shows the digestion with thrombin, and a '-' shows no step was performed, similarly, for the second step written in the bottom of the gel.

3.2.3 Cryo-EM data processing

The fraction loaded on the gel (Figure 24 B) was used for the cryo-EM grid preparation. The concentration estimated by Bradford's assay was 0.19 mg/ml. The procedure for the data collection is given in the methods (Section 2.8). The micrograph showed the presence of a proteins of elongated shape. Below are the 2D classes obtained from template-based picking. The total number of 2D classes selected were 10, consisting of all together 11,291 particles (Figure 26 B). In these 2D classes, the presence of a two protein complex can be seen as "Y" shape. Here, the number of particles were very less, to build an ab-initio reconstruction. Further, data processing and data collection is required to get structure of the complex.

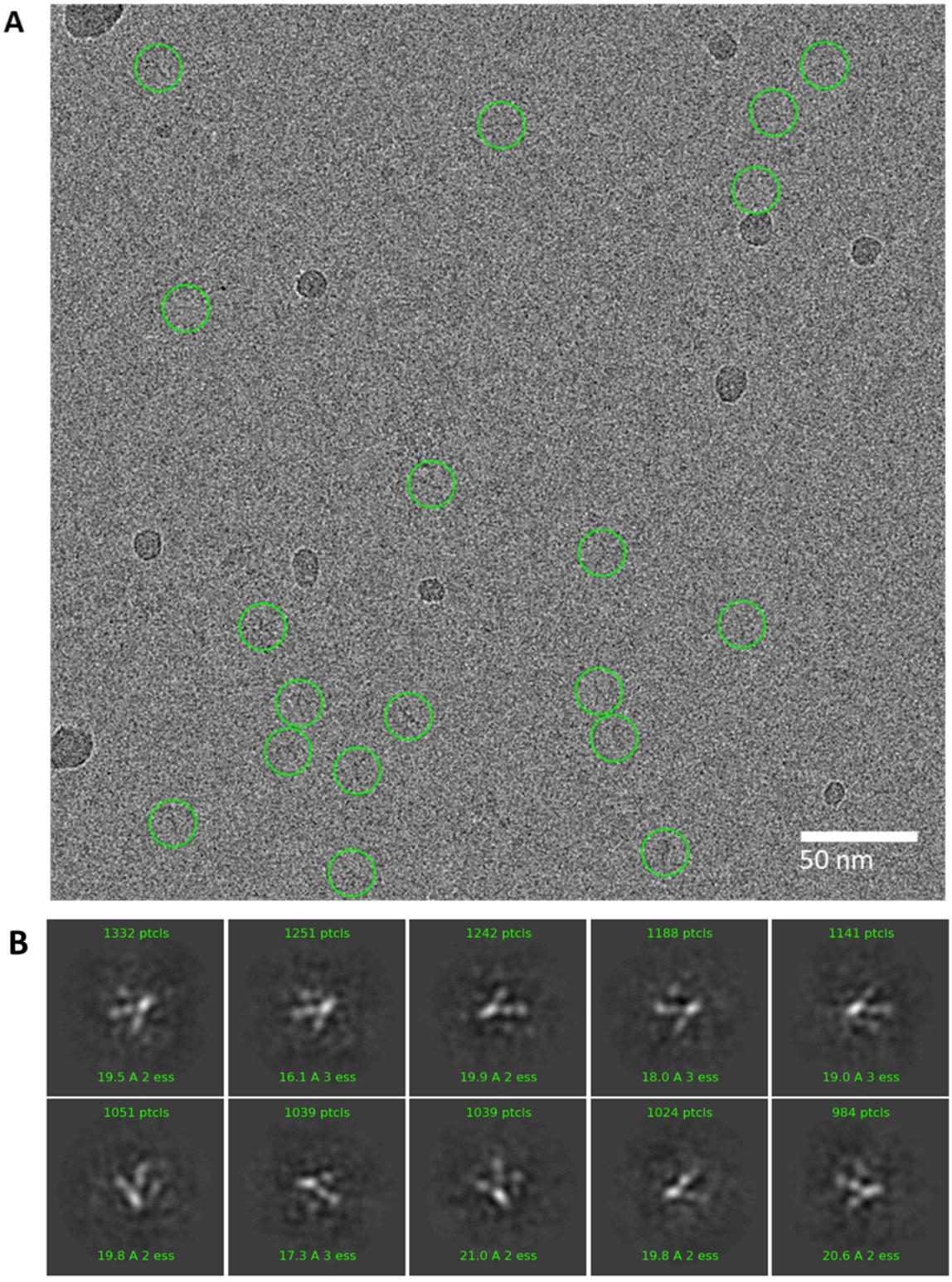

Figure 26. Cryo-EM data processing. A) Sample micrograph showing elongated protein; green circles have a diameter of 200 Å B) Ten 2D classes showing protein complex

4. Discussion and Future prospects

Nup93 interacts dynamically in the NPC through its unstructured and structured region. Previous reports suggest the interaction of Nup93 with multiple proteins in the NPC. The complex formation of Nup93 with Nup155 is crucial to hold the NPC intact as the Nup93 is also responsible for positioning the Channel Nucleoporin Trimer. The NPC has to undergo different conformations to transport the cargo, such as constricted and dilated. These proteins contain multiple interaction sites essential for the assembly and proper functioning of the NPC. The current data in the lab shows that different regions of Nup93 and Nup155 interact to form a complex. We also conducted a study on two complexes as addressed in the result. For the $Nup155^{1-515}$.$Nup93^{599-819}$ complex multiple optimisations were performed to increase the yield and purity of the complex. Finally, an optimised protocol was used to purify the complex. The $Nup155^{1-515}$.$Nup93^{599-819}$ complex was found to be a transient complex, because during the tandem affinity the complex seems to be stable, but disintegrated after the size exclusion chromatography. Additionally, more biochemical studies are necessary to calculate exact affinity values for this complex. Further optimisations, such as chemical cross-linking, is required to stabilise the complex for structure determination using cryo-EM. For the $Nup155^{864-1391}$.$Nup93^{1-819}$ complex, the interaction studies were performed, and the complex was observed both after GST affinity purification and also with the tandem Ni-NTA affinity purification. The presence of the complex was also confirmed with the size exclusion chromatography and western blotting. However, the band intensity of $Nup155^{864-1391}$ after size exclusion chromatography was significantly less compared to the $Nup93^{1-819}$ on the SDS-PAGE gel. It suggested that the complex was not stable without DDM conditions. After using DDM, both protein band intensity was equal after affinity and size exclusion chromatography. After screening of various purification strategies, GST affinity chromatography was selected as the best. The cryo-EM data collected for the sample after GST affinity. For this data set, the preliminary data processing was performed. The 2D classes revealed the presence of a protein complex with “Y” shape. Further data processing need to be done to get the 3D structure of the complex. The high resolution structure will give a better idea of the conformation of the Nup155.Nup93 complex compared to the currently existing 12.6 Å NPC tomogram.

5. References

Aitchison, JD, Suprapto, A, Hjertaas, K, Zhao, Y, and Chait, BT (2000). The Yeast Nuclear Pore Complex: Composition, Architecture, and Transport Mechanism. Journal of Cell Biology 148, 635–652.

von Appen, A, Kosinski, J, Sparks, L, Ori, A, DiGuilio, AL, Vollmer, B, Mackmull, M-T, Banterle, N, Parca, L, Kastritis, P, *et al.* (2015). In situ structural analysis of the human nuclear pore complex. Nature 526, 140–143.

Belgareh, N, Rabut, G, Baï, SW, van Overbeek, M, Beaudouin, J, Daigle, N, Zatsepina, OV, Pasteau, F, Labas, V, Fromont-Racine, M, *et al.* (2001). An evolutionarily conserved NPC subcomplex, which redistributes in part to kinetochores in mammalian cells. J Cell Biol 154, 1147–1160.

Bui, KH, von Appen, A, DiGuilio, AL, Ori, A, Sparks, L, Mackmull, M-T, Bock, T, Hagen, W, Andrés-Pons, A, Glavy, JS, *et al.* (2013). Integrated structural analysis of the human nuclear pore complex scaffold. Cell 155, 1233–1243.

Chopra, K, Burdak, B, Sharma, K, Kembhavi, A, Mande, SC, and Chauhan, R (2020). CoRNeA: A Pipeline to Decrypt the Inter-Protein Interfaces from Amino Acid Sequence Information. Biomolecules 10.

Denning, DP, Patel, SS, Uversky, V, Fink, AL, and Rexach, M (2003). Disorder in the nuclear pore complex: The FG repeat regions of nucleoporins are natively unfolded. Proceedings of the National Academy of Sciences 100, 2450–2455.

Eibauer, M, Pellanda, M, Turgay, Y, Dubrovsky, A, Wild, A, and Medalia, O (2015). Structure and gating of the nuclear pore complex. Nat Commun 6, 7532.

Huang, G, Zhan, X, Zeng, C, Liang, K, Zhu, X, Zhao, Y, Wang, P, Wang, Q, Zhou, Q, Tao, Q, *et al.* (2022). Cryo-EM structure of the inner ring from the Xenopus laevis nuclear pore complex. Cell Research 32, 451–460.

Izaurralde, E, Kutay, U, von Kobbe, C, Mattaj, IW, and Görlich, D (1997). The asymmetric distribution of the constituents of the Ran system is essential for transport into and out of the nucleus. EMBO J 16, 6535–6547.

Jarnik, M, and Aebi, U (1991). Toward a more complete 3-D structure of the nuclear pore complex. J Struct Biol 107, 291–308.

Jumper, J, Evans, R, Pritzel, A, Green, T, Figurnov, M, Ronneberger, O, Tunyasuvunakool, K, Bates, R, Žídek, A, Potapenko, A, *et al.* (2021). Highly accurate protein structure prediction with AlphaFold. Nature 596, 583–589.

Kosinski, J, Mosalaganti, S, Appen, A von, Teimer, R, DiGuilio, AL, Wan, W, Bui, KH, Hagen, WJH, Briggs, JAG, Glavy, JS, *et al.* (2016). Molecular architecture of the inner ring scaffold of the human nuclear pore complex. Science 352, 363–365.

Lin, DH, and Hoelz, A (2019). The Structure of the Nuclear Pore Complex (An Update). Annu Rev Biochem 88, 725–783.

Lin, DH, Stuwe, T, Schilbach, S, Rundlet, EJ, Perriches, T, Mobbs, G, Fan, Y, Thierbach, K, Huber, FM, Collins, LN, *et al.* (2016). Architecture of the symmetric core of the nuclear pore. Science 352, aaf1015.

Lutzmann, M, Kunze, R, Buerer, A, Aebi, U, and Hurt, E (2002). Modular self-assembly of a Y-shaped multiprotein complex from seven nucleoporins. The EMBO Journal 21, 387–397.

Matsuura, Y (2016). Mechanistic Insights from Structural Analyses of Ran-GTPase-Driven Nuclear Export of Proteins and RNAs. J Mol Biol 428, 2025–2039.

Michael J Matunis, JMC (2002). Proteomic analysis of the mammalian nuclear pore complex. J Cell Biol.

Mosalaganti, S, Obarska-Kosinska, A, Siggel, M, Taniguchi, R, Turoňová, B, Zimmerli, CE, Buczak, K, Schmidt, FH, Margiotta, E, Mackmull, M-T, *et al.* (2022). AI-based structure prediction empowers integrative structural analysis of human nuclear pores. Science 376, eabm9506.

Nakano, H, Wang, W, Hashizume, C, Funasaka, T, Sato, H, and Wong, RW (2011). Unexpected role of nucleoporins in coordination of cell cycle progression. Cell Cycle 10, 425–433.

Ori, A, Banterle, N, Iskar, M, Andrés-Pons, A, Escher, C, Khanh Bui, H, Sparks, L, Solis-Mezarino, V, Rinner, O, Bork, P, *et al.* (2013). Cell type-specific nuclear pores: a case

in point for context-dependent stoichiometry of molecular machines. Mol Syst Biol 9, 648.

Palancade, B, and Doye, V (2008). Sumoylating and desumoylating enzymes at nuclear pores: underpinning their unexpected duties? Trends Cell Biol 18, 174–183.

Petrovic, S, Samanta, D, Perriches, T, Bley, CJ, Thierbach, K, Brown, B, Nie, S, Mobbs, GW, Stevens, TA, Liu, X, *et al.* (2022). Architecture of the linker-scaffold in the nuclear pore. Science 376, eabm9798.

Rasala, BA, Ramos, C, Harel, A, and Forbes, DJ (2008). Capture of AT-rich chromatin by ELYS recruits POM121 and NDC1 to initiate nuclear pore assembly. Mol Biol Cell 19, 3982–3996.

Rexach, M, and Blobel, G (1995). Protein import into nuclei: association and dissociation reactions involving transport substrate, transport factors, and nucleoporins. Cell 83, 683–692.

Ridley, RG (1989). Antibodies: A Laboratory Manual. Edited by Ed Harlow and David Lane. Cold Spring Harbor: Cold Spring Harbor Laboratory. New York. 1988. 726 pages. Paper $50.00. ISBN 0 87969 314 2. Genetical Research 54, 161–161.

Sakuma, S, and D'Angelo, MA (2017). The roles of the nuclear pore complex in cellular dysfunction, aging and disease. Seminars in Cell & Developmental Biology 68, 72–84.

Sangeeta Niranjan, Jyotsana Singh, and Radha Chauhan (2021). Cryo-EM structure of human Nup155 reveals the biochemical basis for atrial fibrillation linked genetic mutation R391H. bioRxiv, 2021.10.05.463194.

Stuwe, T, Bley, CJ, Thierbach, K, Petrovic, S, Schilbach, S, Mayo, DJ, Perriches, T, Rundlet, EJ, Jeon, YE, Collins, LN, *et al.* (2015). Architecture of the fungal nuclear pore inner ring complex. Science 350, 56–64.

Zhang, X, Chen, S, Yoo, S, Chakrabarti, S, Zhang, T, Ke, T, Oberti, C, Yong, SL, Fang, F, Li, L, *et al.* (2008). Mutation in nuclear pore component NUP155 leads to atrial fibrillation and early sudden cardiac death. Cell 135, 1017–1027.

Zuccolo, M, Alves, A, Galy, V, Bolhy, S, Formstecher, E, Racine, V, Sibarita, J-B, Fukagawa, T, Shiekhattar, R, Yen, T, *et al.* (2007). The human Nup107-160 nuclear pore subcomplex contributes to proper kinetochore functions. EMBO J 26, 1853–1864.